ABSTRACT

THOPPEY MUTHURAMAN, NAGARAJAN. Development and Optimization of an Alternative Electrospinning Process for High Throughput. (Under the direction of Dr. Russell E. Gorga and Dr. Laura I. Clarke).

This work is an investigation of the prospect of electrospinning from the simplest aperture-free system, a flat plate on which polymer solution is placed as droplets or undergoes a gravity-assisted flow. Nanofibers with a similar fiber diameter and diameter distribution were fabricated at similar voltages and working distances as that in an aperture-based system, however with much more flexibility to scale up the process and with no openings or nozzles that can clog. It is verified that the field gradient at the site of jet formation is important. In particular, it is shown that the relatively homogeneous electric field on the plate surface does not promote electrospinning as compared with the significantly more inhomogeneous field at the needle tip in the needle-plate configuration. However, the strong field gradient at the plate edge allows electrospinning from unconfined droplets of the polymer solution and formation of fibers with very similar diameters and diameter distributions as those fabricated by traditional needle electrospinning for the same polymer solution. Further it is also shown that this edge-plate methodology can be extended to systems with many "edges" and curved edges (such as those from a hollow cylinder) for massively-parallel electrospinning (that is, higher potential throughput). A detailed examination of the changes in fiber diameter, diameter distribution, and mat porosity is reported as a function of the electric field magnitude and geometry, and it is concluded that the process is quite stable over a range of experimental conditions. The connection between fiber properties and spinning conditions via changes in the length and duration of the linear region and the degree of whipping is

discussed in the context of comparing edge-plate and needle-plate electrospinning. Not only do these results address issues specific to such a surface-based, parallel aperture-less electrospinning approach, they also continue to expand understanding of electrospinning in more general terms.

Development and Optimization of an Alternative Electrospinning Process for High Throughput

by
Nagarajan Thoppey Muthuraman

A thesis submitted to the Graduate Faculty of
North Carolina State University
in partial fulfillment of the
requirements for the degree of
Master of Science

Textile Engineering

Raleigh, North Carolina

2010

APPROVED BY:

Dr. Russell E. Gorga Committee Chair	Dr. Laura I. Clarke Co – Chair
Dr. Maury Balik Minor Representative	Dr. Jason Bochinski Committee Member

DEDICATION

To *mom* – Ms. Pushpavalli Thoppey Muthuraman

BIOGRAPHY

Nagarajan Thoppey Muthuraman was born on July 12th, 1978 in the city of Madurai, India. He obtained his Diploma in Textile Technology in 1996 from the State Board of Technical Education in Chennai, India. He worked as a production executive in Coats India Limited, a spun-yarn manufacturing company in Tuticorin, India for four years. He obtained a Bachelors of Textile Technology in 2004 from University of Madras, Chennai, India in the following three years. After his graduation, he worked as a compliance auditor and product development assistant for Epic Designers Private Limited, an apparel manufacturer in Dhaka, Bangladesh for two and a half years.

Nagarajan joined the department of Textile Engineering, Chemistry and Science at North Carolina State University in the Spring of 2008 for a Masters in Textile Engineering. Since then, he has worked with Dr. Russell E. Gorga and Dr. Laura I. Clarke on developing a high throughput electrospinning process. Following the completion of his Masters, Nagarajan plans to continue working in the field of electrospinning and earn a Doctorate of Philosophy in Fiber and Polymer Science under the direction of Dr. Russell E. Gorga and Dr. Laura I. Clarke.

ACKNOWLEDGEMENTS

I would like to express my sincere gratitude to Dr. Russell E. Gorga and Dr. Laura I. Clarke for their constant support and encouragement during this research work. Dr. Gorga has been an incredible mentor and great source of inspiration. He has been always there to point out the right direction, whenever and wherever I needed. I would like to thank Dr. Jason Bochinski for his valuable guidance in this research. I am indebted to Dr. Clarke and Dr. Bochinski for nurturing and developing the scientist within me. It has been a wonderful experience to learn from all of them. I take this opportunity to thank all of their support and patience especially in the process of documenting this work. I also thank Dr. Maury Balik for agreeing to be in the committee as a minor representative.

I submit my sincere thanks and appreciation to Mr. Hai Bui and Mr. Dzung Nguyen (Win) for their daily assistance. I acknowledge all my lab mates especially Beth, Kelly, Erik, Remya, Rebecca and Mary for their help and fruitful discussions. I am thankful to Mr. Chuck Mooney (AIF) and Mrs. Judy Elson for training me on the Scanning Electron Microscope. I would like to thank Ms. Angie Brantley for her help and coordination from day one.

I would like to acknowledge my sister Usharani T Ganesh for being instrumental in achieving my dreams. I lack the words to adequately express my heartfelt gratitude to all my sisters for their prayers which keep me well wherever I am. Also, I thank all my friends back in India especially Balakumar, Sivakumar, and Ravikumar who keep me laughing loud, though I am away from home.

Life here in the United States would not have been so enjoyable or cheerful without great people around me. I feel immense pleasure to acknowledge and thank all of them especially Mridula, Vamsi, Anjali, Anita, and my aunt and cousins. I would be remiss if I did not acknowledging Krishna Bala for her unconditional love and support in making this journey so cheerful and meaningful.

TABLE OF CONTENTS

LIST OF FIGURES

LIST OF TABLES

Chapter 1

Introduction

Polymeric nanofibers can be fabricated by a number of techniques such as drawing, template synthesis, phase separation, self-assembly, and electrospinning [1]. In drawing, a micropipette is dipped into the droplet near the contact line and then withdrawn from liquid at a speed of approximately 1 X 10^{-4} ms^{-1}, resulting in nanofibers in the range of 2 nm to 100 nm. In template synthesis, a porous membrane is used as a template onto which the polymer solution is applied with pressure. This causes extrusion of the polymer solution and when it comes in contact with a solidifying solution it gives rise to nanofibers. In this technique, fibers in the range of 100 nm can be obtained. In the phase separation technique, as the name implies, the polymer is initially mixed with an incompatible solvent and then the solvent is extracted to leave behind a nanofibrous polymer structure. A porous structure in the range of 50 – 500 nm can be produced. In self-assembly, small molecules are arranged in a concentric manner by intermolecular forces such that bonds form between them. Typical fiber diameters are in the range of 7 nm to 100 nm. In electrospinning, an electrostatic force causes a polymer droplet (in the melt or solution) to initiate a jet that travels linearly for certain distance and undergoes multiple whipping instabilities that elongate the jet (and cause solvent evaporation-in the case of a solution) to give nanofibers which are deposited on a grounded collector plate. In this technique continuous fibers in the range of 100 – 500 nm can be produced. Table 1.1 [1] compares these techniques from a processing point of view.

Table 1.1 Comparison of processing techniques for obtaining nanofibers (taken from [1])

Process	Current use (level of technology)	Can the process be scaled?	Repeatability	Convenient to process?	Control of Dimension
Drawing	Laboratory	No	Yes	Yes	No
Template Synthesis	Laboratory	No	Yes	Yes	Yes
Phase Separation	Laboratory	No	Yes	Yes	No
Self-Assembly	Laboratory	No	Yes	No	No
Electrospinning	Laboratory (with potential for industrial processing)	Yes	Yes	Yes	Yes

Of all the techniques, electrospinning is the most common and a relatively simple technique for nanofiber fabrication [1-6]. Nanofibers with diameters of 40 – 1000 nm can be produced from polymer solutions or melts and collected as nonwoven mats with ~70-80% porosity. With small modifications to the electrospinning apparatus, fibers with uni-axial arrangement can be obtained.

Electrospun nanofibers have significant technological promise due to their high surface area to volume ratio and the resultant nanofibrous mats are lightweight due to their high porosity. Figure 1.1 shows many potential applications of polymeric nanofibers. The high relative surface area has the potential to facilitate catalysis and other sensitive surface reactions or to enable highly sensitive sensors [1]. For example, humidity sensors based on a

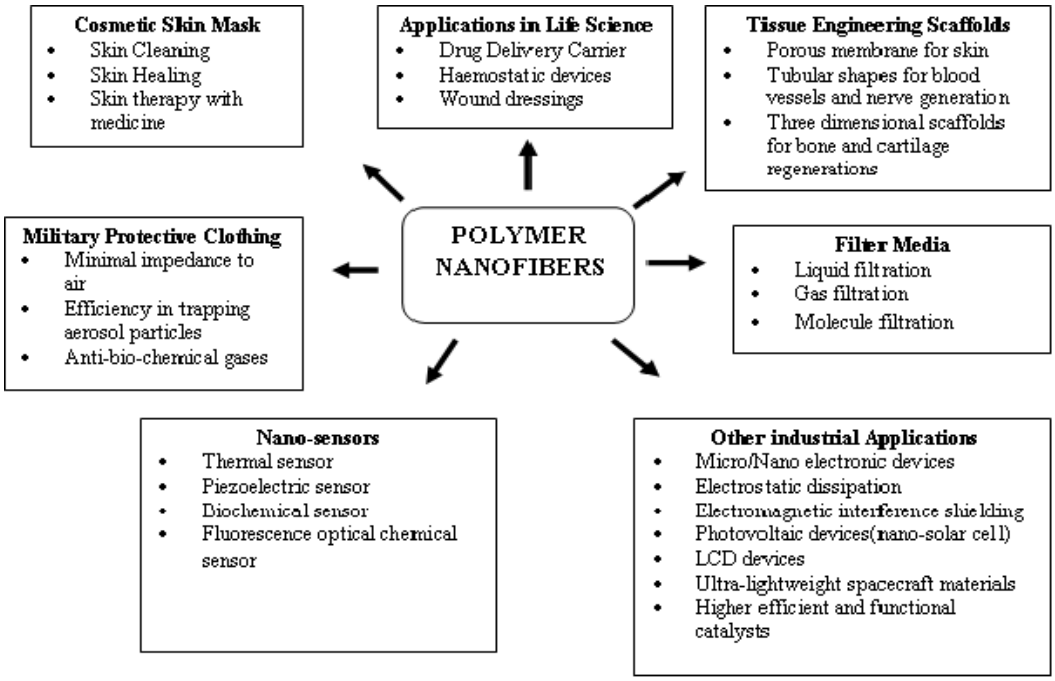

Figure 1.1 Potential applications of nanofibers [3]

PEO nanofiber carrying 1 wt% of LiClO4 showed a sensitivity level six times that of comparable thin-film material [7]. Nanofibrous materials doped with conductive particles have shown excellent conductivity [8]. Such materials are well suited for conductive sensor applications. If the nanofibrous material (doped with a conductive particle) were to come in contact with a chemical and/or biological agent that could swell the fiber, the volume of the material would increase (due to the swelling) which in turn would disrupt the connectivity of the conductive particle. This, in turn, could alter the nanofibrous mat's electrical resistance. Although this phenomenon is already utilized in electronic-nose technology using polymer films [9], nanofibrous mats are efficient because of their high specific surface area.

The nanofiber diameter and porosity are well-suited for medical applications such as tissue scaffolds, drug delivery devices, and wound protection [4, 10]. The success of polymer nanofibrous mats in tissue scaffold applications occurs primarily because the fiber diameters and overall porosity (and pore size) are on the same scale as the structural features present in body tissue environments (i.e. the extracellular matrix). The ultimate goal will be to seed nanofibrous scaffolds with cells that can grow and differentiate *in vitro* or *in vivo* to replace damaged tissue. Bio-degradable polymer nanofibers play an important role in such applications.

High porosity and micro-scaled pore size provide high filtration efficiency and have enabled applications of nanofibrous materials within the liquid and air filtration industries [10, 11]. Electrospun nanofiber coatings can be directly applied to open cell polyurethane foam (for applications that require high air flow resistance) resulting in relatively high filtration efficiency. Besides industrial applications for these membranes, they can also be used to filter moisture and dust (in HVAC systems). Unclean air which contains bacteria could also be purified using these membranes: chemical modification could be used to deactivate specific bacteria, thereby creating new multifunctional (and responsive) membranes. Further, since these membranes are light weight they could be used for protective clothing applications, which require high flexibility, breathability, elasticity, drapability, and filtration efficiency (for face masks).

In addition, nanofibrous scaffolds doped with conductive particles have been shown to perform as strain sensors (functioning much like the conductive sensors described above) [12]. Other important potential applications of nanofibers with conductive particles include intelligent and communicative textile structures, smart analyte vapor sensors for defense and security applications, environmental and medical diagnostics, self-reporting smart structures, and, in particular, self-reporting filtration media.

However, despite their utility, wide-spread industrial implementation of electrospun nanofibers is limited by low fabrication rates (0.01 – 0.1 g/hr) in the traditional electrospinning configuration, where the nanofiber source is a single jet arising from a needle aperture through which polymer solution is extruded. Numerous approaches to "scale-up" the fabrication rate of electrospun materials [13] have been reported, which are discussed in detail in the background section. In brief, these techniques can be summarized as 1) spinning from multiple apertures; 2) generating multiple jets from each aperture; or 3) generating jet sites without apertures; for instance, from the cylindrical surface in the commercial Nanospider^{TM} [11] or from sharp spikes formed when metallic liquid is manipulated by electric and magnetic fields [14]. Each system has its own merits and drawbacks. Generally, in aperture systems, the average nanofiber diameter and diameter distribution is smaller, however they are prone to clogging and the system is quite complex (with multiple apertures). On the other hand, aperture-free systems are typically free of clogging; however the average nanofiber diameter and diameter distribution are often significantly larger than

those from the more traditional (i.e., aperture-based) approaches. Thus, in aperture-free systems, with increased throughput the preferred fiber morphology may be compromised.

This work investigates the prospect of electrospinning from a particularly simple aperture-free system which can fabricate nanofibers similar or superior to that of traditional needle electrospinning with respect to average diameter, diameter distribution and mat porosity yet has a greater potential for scaling up to higher throughput without the possibility of clogging.

Chapter 2

Background

2.1 Introduction

This chapter will provide a comprehensive overview of fundamentals of the electrospinning process and other elements that will be introduced in the later chapters. Section 2.2 provides a historical overview of electrospinning while section 2.3 focuses on the apparatus. Section 2.4 outlines various variables involved in the electrospinning process. Section 2.5 reviews the approaches so far attempted in scaling up the process. Finally, sections 2.6 and 2.7 provide an overview of self-assembled monolayers and electrostatic simulation respectively.

2.2 Historical overview

Electrospinning is a simple, versatile technique which has been used for more than a century now. However, a tremendous increase in number of research activities utilizing this technique has occurred in just over the last two decades. Historically, electrostatic interactions on liquids were observed in 1600s by William Gilbert. Such an observation turned out to be a technique to produce nanofibers from liquids through significant contributions from Nollet (1749), Morton (1902), Cooley (1902), and Zeleny (1914). Formhals, commonly recognized as the father of present day electrospinning technology through his various patents (1934 – 1944) [5, 15-18], primarily focused on different methods or set-ups of producing nanofibers using electrostatic forces.

Baumgarten (1971) [19] reported comprehensive experiments on the electrostatic spinning of acrylic microfibers from solution, and published many state-of-the-art stop-motion photographs of electrospinning jets. A decade later Larrondo and Manley [20] published their works on electrospinning from polymer melts. A large break in the progress of research from 1944 to 1971 is believed to be due to the absence of industrial initiatives or applications for such nanofibrous materials. Applications of electrospun nanofibers became apparent when Donaldson Co., Inc., (USA) introduced their first commercial product (filters) in 1981 and a widespread interest was created across many research fields. (It is germane to note, however, that it is also reported [21] that a team in the USSR (Rosenblum and Petrianov-Sokolov) helped establishing the first known industrial facility for producing fibrous materials for military gas masks.) More recently, research on the process of electrospinning received a great deal of academic attention over the last decade, once Reneker and coworkers [22-24] spun various kinds of polymers and characterized their properties. Since then, the number of research publications has grown exponentially in the past 15 years and continues to do so.

2.3 Apparatus

Electrospinning in the most familiar implementation utilizes a high electric potential difference applied between a charged needle (through which a fluid is pumped by a syringe pump) and a flat collector plate (as shown in Figure 2.1). (Here we refer to such a needle-plate arrangement as *traditional needle electrospinning* (TNE)). The polymer solution emerging from the needle is charged and the electrostatic forces propel the fluid through the

electric field toward the grounded collector plate. Under optimized conditions (i.e., polymer concentration, applied electric potential, distance between needle and the collector, and solution flow rate), the jet follows a linear path for a few centimeters past the tip of the needle and then undergoes multiple instabilities, resulting in a whipping region where the solvent evaporates as the fiber is elongated. On average, the diameter of the jet reduces by 10,000 times in a short (typically ~15 cm) distance between the tip of the needle and collector plate. This whipping action results in solvent-free polymer nanofibers, which are usually on the order of 100 nanometers in diameter, deposited on the collector plate. The TNE process is simple, cost effective, and suitable for wide range of polymers in either solution or the melt phase.

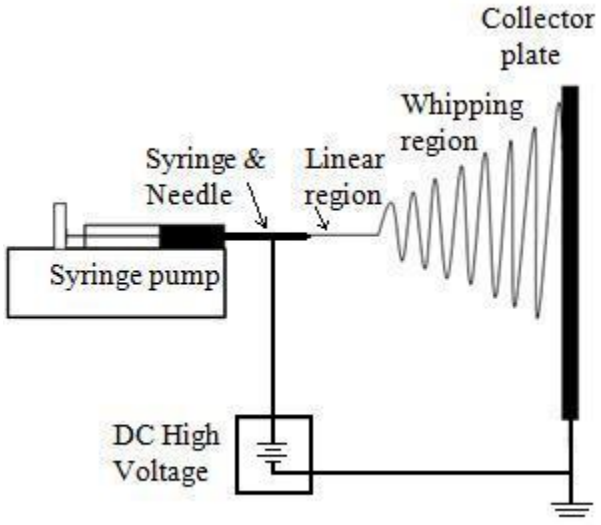

Figure 2.1 Schematic diagram of traditional needle electrospinning (TNE)

Numerous modifications in the TNE set-up have been investigated in order to achieve (or attempt to achieve) enhanced properties and collection methods of nanofibers. These modifications are discussed below by classifying the basic set-up in to three zones, namely: i) the feed zone; ii) the spinning zone; and, iii) the collection zone.

i) Feed zone (from the reservoir to the needle tip in TNE): The aim of the feed zone is to continuously provide a fluid that results in the formation of a fine, electrically charged droplet (upon applying electric field) for the electrospinning process. Modifications in the feed zone include different needle designs (single and bicomponent needles [25, 26], multiple needles (discussed in 2.7)), different electrode designs (needle with flat plate or cylindrical electrodes [27, 28]), and the addition of external systems like an air-blower that assists in the evaporation process [29]. These modifications help in altering the morphology (and, in some cases, the throughput) of the final fiber collected in the collection zone.

ii) Spinning zone (located between the needle tip to the collector plate in TNE): The purpose of this region is to reduce the diameter of the jets via the whipping instability (as described above) and evaporate the solvent (in the case of solution processes). Only a few modifications, like using cylindrical electrodes to control the spinning region, in this zone have been reported so far [30, 31]. These modifications were adopted to manipulate the whipping region in order to control the fiber diameter or deposition on to the collector.

iii) Collection zone (collector surface): The object of this zone is to gather nanofibers from the spinning zone by providing a suitable (usually grounded) potential surface. A number of modifications [32-34] in this zone have been explored in order to obtain different structures (such as yarns, mats, wound filaments, or conduits) or different alignments of the fibers in a plane (such as random, parallel, or pseudo-woven).

All these modifications are designed to obtain different forms of nanofibrous materials or different morphologies while the overall electrospinning process remains the same. A detailed description of fundamental physics behind the electrospinning process is discussed in the following section.

2.4 Physical description of the electrospinning process

In electrospinning, when an electrostatic force is applied to a pendent droplet (usually polymer solution), the droplet deforms to form a conical shape commonly called a Taylor cone [35]; when the electrostatic force overcomes the surface tension of the droplet, a jet is initiated from the vertex of the conical droplet and travels towards the collector (ground potential). From the vertex, the jet travels in a straight line for a finite distance that is referred to as the linear region. At the end of linear region, the jet starts following a helical path forming a conical shape and the cone increases in size as it approaches the collector. This is due to multiple instabilities and this region is referred as the whipping region. In this region, the diameter of the jet decreases several orders of magnitude and the solvent evaporates,

finally leaving dried nanofibers on the collector. The physical characteristics of the electrospinning process can be described by these three regions, namely, the Taylor cone, the linear region, and the whipping region [23, 36].

2.4.1 Taylor cone

In 1969, Taylor studied the deformation of liquid bodies upon application of an electric field and observed that at a critical electric field, a polymer droplet deforms and gives rise to a conical shape [35]. The conical shape occurs as a result of charge repulsion within the liquid and surface tension mechanisms [23, 37]. This conical shape was later referred to by other researchers as the "Taylor cone". The vertex of the cone, where the jet emanates, is an interesting area to study for many researchers as there is a difference in the velocity of the jet before (usually, the feed rate) and after (the drawing rate, that depends on the electric potential) the vertex. These velocity gradients help in stabilizing the electrospinning process.

Fang et al. [38] described the conditions which need to be met in order to emanate a jet from a droplet. Figure 2.2 shows a pendent droplet (white region within the hash-marked region) from a needle (hash-marked region). The surface tension (Y) of the pendent droplet was given in Equation 1 where g is the gravitational constant, $\Delta\rho$ is the density difference between the fluids at the interface ($\Delta\rho = \rho$ for the droplet having a liquid/air interface, where ρ is the density of the fluid), r_o is the radius of curvature at the apex of drop, and β is the shape factor [38].

Electrostatic force (F_s) exerted on the surface of the droplet per unit area is shown in Equation 2, where ρ_s is the surface charge density (per unit area), σ is the conductivity of the fluid and E is the electrostatic field. In order to overcome the surface tension, the condition

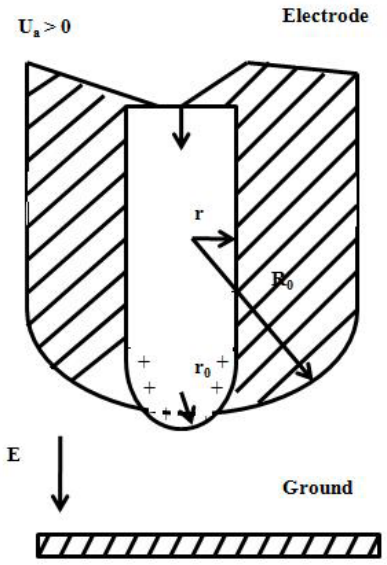

Figure 2.2 Schematic of a droplet from a single needle in an applied electric field [38].

shown in Equation 3 must be met, where ρ_0, V, and g are the density and volume of the droplet and the gravitational acceleration, respectively.

$$Y = g\Delta\rho r_0^2 / \beta \quad (1)$$

$$F_s = \rho_s (\sigma) E \quad (2)$$

$$F_s = \rho_s (\sigma) E \geq Y - \rho_0 V g \quad (3)$$

Once the electric field overcomes the surface tension, the shape of the droplet changes at the tip forming a cone (Taylor cone) and a small jet of liquid is emitted from the cone vertex [38]. Taylor showed that a cone angle of 49.3º was observed when a critical point is reached to disturb the equilibrium of the droplet at the tip of the capillary. In a recent study, Yarin et al. [39] have shown that the cone angle specified by Taylor is based on a spheroidal approximation, and there could be other shapes based on hyperboloidal approximations for which a cone angle of 33.5º was observed. These results suggested that Taylor cone angle varies with the polymer solution but it would be in the range of 30 - 50º.

2.4.2 Linear region

The jet initiated from the Taylor cone follows a linear path (with small lateral perturbations) before the onset of bending instabilities. Considering the jet as comprised of multiple (small) segments, the leading segment of the jet is accelerated as the potential difference drives the jet from high potential (needle) toward low potential (collector). Similarly, the leading segment of the jet draws the subsequent segments that are entangled by the surface tension and viscoelastic forces. This drawing results in reduction in diameter. Here viscosity plays an important role in determining the rate of thinning of the jet. The jet remains in equilibrium (maintaining a linear path) until a strong charge repulsion within the jet overcomes the surface tension and viscoelastic forces in the jet [23, 36].

Many models using electrohydrodynamical theories have been applied in order to predict various parameters of the tapered jet. The length of the linear region (L) was given by

Equation 4 [40] where K is the solution conductivity, Q is the feed rate, ρ is solution density, χ is the aspect ratio of the jet, E_α is local electric field strength, I is electric current and έ is the dielectric constant of the polymer.

$$L^5 = \frac{K^4 Q^7 \rho^3 (\ln \chi^2)}{8\pi^2 E_\alpha I^5 (\acute{\varepsilon})^2} \quad (4)$$

$$h = \left(\frac{6\,\eta\, Q^2}{\pi E_\alpha I} \right)^{1/2} z^{-1} \quad (5)$$

At length L, the jet approaches the asymptotic regime where only electrostatic force and inertial force dominate. The diameter of the jet (*h*) at this asymptotic regime is given by Equation 5, where η is the viscosity and z is the axial coordinate [40]. It should be noted that the linear region (L) and the terminal diameter (h) of the jet before the instability is directly proportional to the feed rate (Q).

2.4.3 Whipping region

The whipping region consists of multiple bending instabilities and is the most complex part of the electrospinning process. A review from Jaworek et al. [41] focused on the instabilities of electrified jets classifies them into different modes such as dripping, spindle mode, oscillating jet mode, and the precession mode in which the first two modes are relevant to electrospraying while last two modes are relevant to the whipping mode that are found in electrospinning.

The whipping instability in electrospinning can be discussed in two stages; namely, the first order electrical bending instability and the higher order bending instability [36]. While perturbations occur everywhere along the jet path, the instability occurs only at a certain distance away from the tip of the needle as discussed in previous section. This could also be discussed in terms of bending stiffness of the jet. Bending stiffness = YM, where Y is the Young's modulus and M is the second moment of area (or second moment of inertia) which can be written as $M = (\pi/4) R^4$, where R is the jet radius. As the jet radius decreases, the bending stiffness decreases extremely rapidly, thus assisting the onset of the first order bending instability [1].

Reneker et al. [42] described the first order instability using the Earnshaw theorem (Figure 2.3) where three points A, B and C of like charges were considered along the jet axis. Interaction of these three like charges results in a perturbation that moves the point B off the axis (perpendicular to the axis) by a distance δ to B'. Reneker et al. showed that this small perturbation grows exponentially. When this perturbation occurs in a liquid jet, forces such as surface tension and viscoelatic forces attempt to counteract the Coulombic force. However, the Coulombic force dominates,overcoming the viscoelastic forces and surface tension, and thus allows the perturbation to grow as a first order instability.

Now the jet follows a helical path around the axis of the jet and grows in size as it approaches the collector. While this first order instability grows further, multiple instabilities establish in a similar manner, but at a much smaller scale, than the first one, as shown in

Figure 2.4. Reneker and Fong [43] presented a prototypical path that the jet follows during its multiple instabilities and showed that the instability follows a cycle of three steps: (1) a smooth segment that is linear or curvilinear suddenly dislocates (bends) from its path due to small perturbation; (2) the segment of the jet within the bend region extends and the jet follows a helical path with increasing diameters; and, (3) as the perimeter of the loops increase, the cross-sectional diameter of the jet grows smaller; and hence, the conditions for step (1) are re-established on a smaller scale, thus the next cycle of bending instabilities begins. Consequently, as a result of multiple instabilities, the jet elongates and the diameter of jet reduces considerably; while doing so, the jet solidifies and ultimately deposits on the collector as a dried nanofiber.

2.5 Electrospinning variables

There are a number of research publications [1,28,44-59] that have studied the effect of variables affecting electrospun fibers and/or mat quality. Figure 2.5 shows a general classification of these variables as: (1) material variables; (2) process variables; and (3) equipment variables. Each variable affects the electrospinning process in one or more ways, and therefore can affect the final fiber quality. In this section, the variables that have significant effect on fiber quality are discussed.

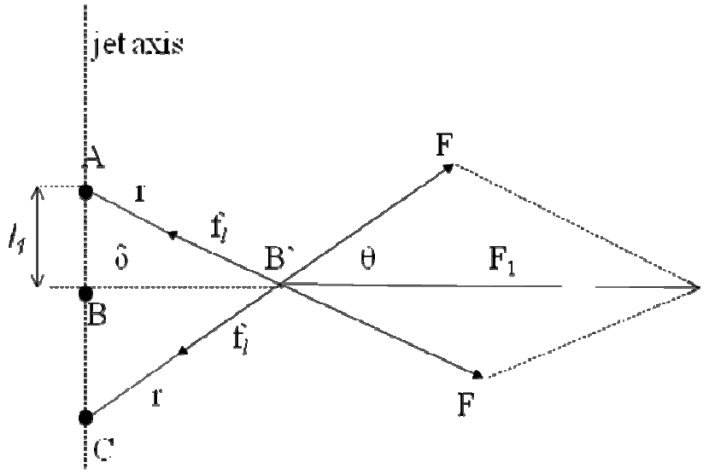

Figure 2.3 Illustration of Earnshaw instability, leading to bending of an electrified jet [42].

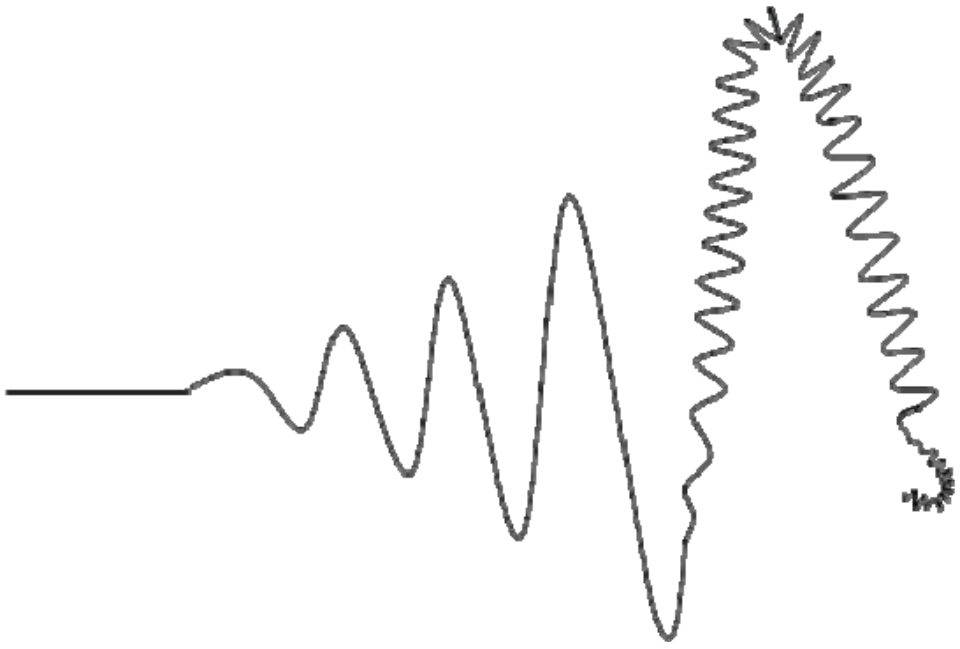

Figure 2.4 Representation of multiple instabilities from a single jet

2.5.1 Material variables

2.5.1.1 Polymer concentration and molecular weight

Higher polymer concentration in solution increases the molecular entanglements which raises the bending stiffness of the jet. This stiffness prevents the jet from whipping until thinner diameter jets are established and therefore, lengthens the linear region for the jet. Thus, for a fixed working distance, the whipping region is reduced in size, resulting in a larger fiber diameter (and a smaller area of deposition on collector plate). Conversely, the fiber diameter will decrease with lowering of the polymer concentration, however below some minimum concentration level, the jetting process is not stable and a bead-like morphology is observed [44]. This beading occurs because at lower polymer concentration, there are not enough entanglements between polymer chains to create continuous, uniform fibers. The effect of molecular weight is similar to the concentration, where polymer solutions of higher molecular weight have more entanglements, thus resulting in larger diameter fibers [30, 45, 46, and 60].

2.5.1.2 Solution conductivity

Solution conductivity reflects the charge density in the solution, thus affecting the charge repulsion in the solution and so the elongation level of a jet by an applied electrical force. Under identical processing parameters, a solution with higher electrical conductivity would have stronger charge repulsion due to more charge density and may be subjected to greater bending instabilities (higher elongation) resulting in fibers with smaller diameters (and an increased surface area (deposition) of fibers on the collector plate). In other words, with

increased solution conductivity a lower applied voltage would be sufficient to initiate a jet. Solution conductivity can be altered by the choice of solvent and/or addition of ions or other charged particles [45, 46].

2.5.1.3 Surface tension

Higher surface tension solutions tend to form beaded fibers. The surface tension of the polymer solution drives the jet to break into multiple droplets, while the viscoelastic forces of the polymer solution acts to maintain a continuous or stable jet. When the surface tension is higher than the viscous forces, beaded fibers are produced, similar to the process previously discussed for low concentration solution where beaded fibers were observed when there are not enough polymer chain entanglements (viscous forces). In general, polymer solutions of low surface tension are preferred for electrospinning [1, 38].

2.5.1.4 Other material variables

In addition to the variables listed above, solvent vapor pressure, density of the solution, elasticity [54] are other variables can have a minor effects on the resulting fiber properties [1].

2.5.2 Process variables

2.5.2.1 Applied voltage - Magnitude

The electrospinning process is stable when the collection of fibers (take up) is balanced by the fluid flow rate, for a polymer at some specific voltage.

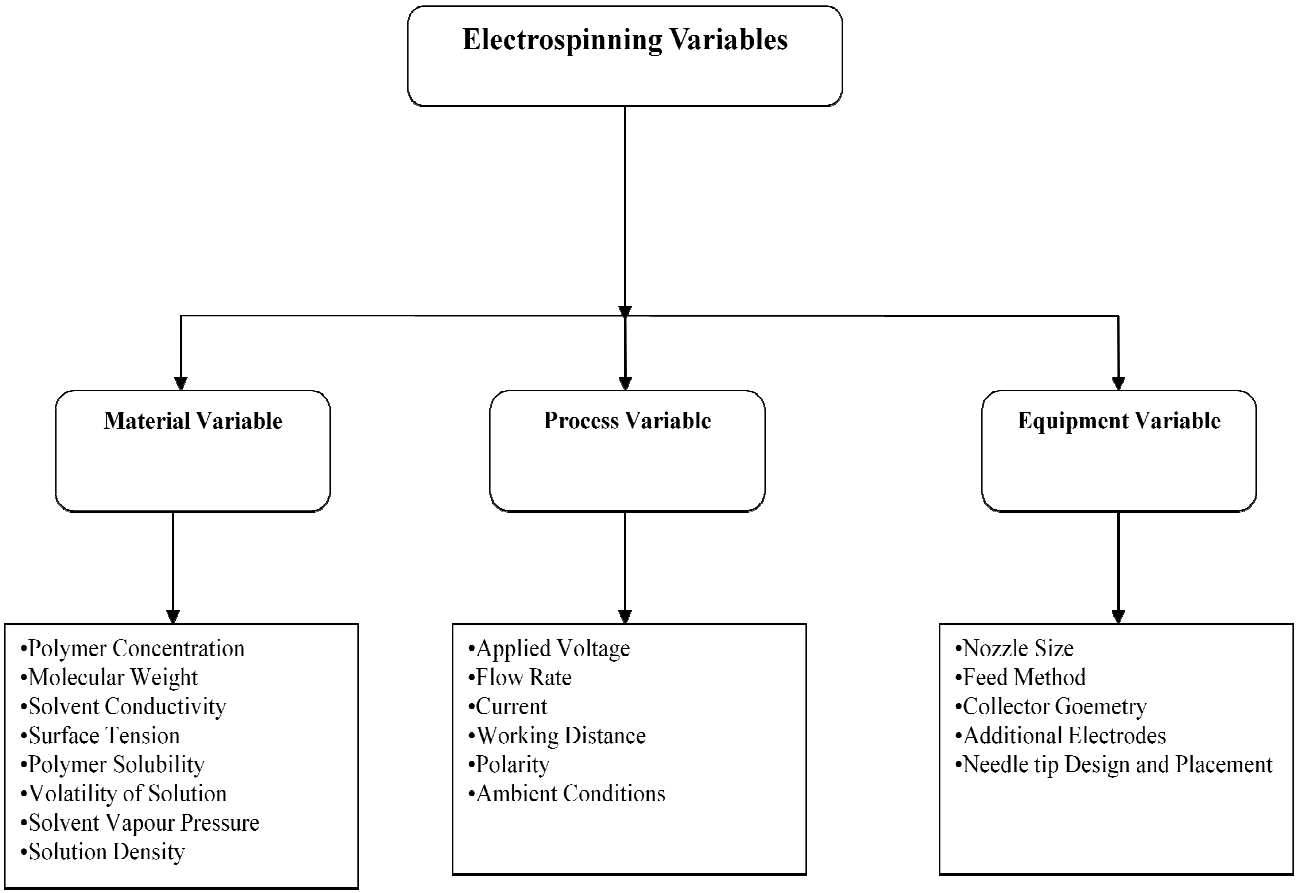

Figure 2.5 Classification of electrospinning variables

Researchers [47, 59] have studied the effect of applied voltage (magnitude) on fiber diameter and observed both increasing and decreasing trends. Increasing the applied voltage draws more fluid from the tip of the needle, thus creating a longer linear region (due to the excess volume of fluid) which results in larger fiber diameters. However, the increased electrical force also increases the whipping instability which raises the frequency of whipping, and thus, counteracts the effect on fiber diameter [28]. In addition, at higher applied voltages multiple jets have been observed, resulting in a larger distribution of fiber diameter. It has also been shown that beaded fibers can be created at increased voltage. At low voltages, less fluid is drawn from the tip of the needle resulting in a shorter linear region and consequently (for a fixed working distance), a longer whipping region [1]. However, the reduced electrical force also decreases the frequency of whipping and counteracts the drawing (elongation) that was expected from the longer whipping region, and hence, (ironically) there is no overall effect on fiber diameter.

2.5.2.2 Applied voltage – Signal and Polarity

Usually a DC high voltage with positive polarity is used in electrospinning. Researchers [55, 56] have observed that the electrospinning process with negative polarity is less efficient and also resulted in beaded and uneven fibers.

Electrospinning with AC potentials are of recent research interest. Researchers have obtained aligned nanofibers in such cases [48, 50, and 53]. Also, AC electric potentials result in

reduced whipping instability [49, 51] which could be usefully applied in obtaining multiple jets and avoiding inter-jet interactions.

2.5.2.3 Volume feed rate

Volume feed rate is an important variable that has a significant effect on fiber diameter. Fiber diameter increases significantly with feed rate. However beyond a certain limit, solvent does not evaporate completely resulting in fused fibers or fibrous mat with residual solvent (and hence "wet" polymer) on the collector. At very high feed rates, polymer droplets would drop from the needle, thereby affecting the stable electrospinning process. At a slow feed rate, there is not enough solution for the electrospinning process, eventually resulting in the production of beaded fibers or beads [45, 47].

2.5.2.4 Working distance

Effect of working distance on the fiber diameter is similar to that of the applied voltage. An optimal working distance is required for a standard electrospinning process. Longer working distance allows the jet to travel more time in the whipping region, which might result in smaller fiber diameter. However, increased working distance reduces the electric field strength (for a fixed applied voltage) which results in a decrease in the frequency of the whipping instability. These phenomena counteract each other and there is little effect on the fiber diameter. Alternatively, a shorter working distance reduces the jet travel time, thereby resulting in unsolidified (i.e., wet) material being deposited on the collector [45, 47].

2.5.2.5 Other process variables

Other process variables such as electric current, ambient conditions (RH (relative humidity), temperature, vacuum) also affect the fiber morphology. Temperature affects the evaporation rate of the solvent and viscosity of the solution thereby affecting final fiber diameter [57]. Effect of RH depends on the polymer that would increase or decrease the fiber diameter. Investigations at vacuum conditions resulted in little effect on mechanical properties of the fibrous mat [51, 52].

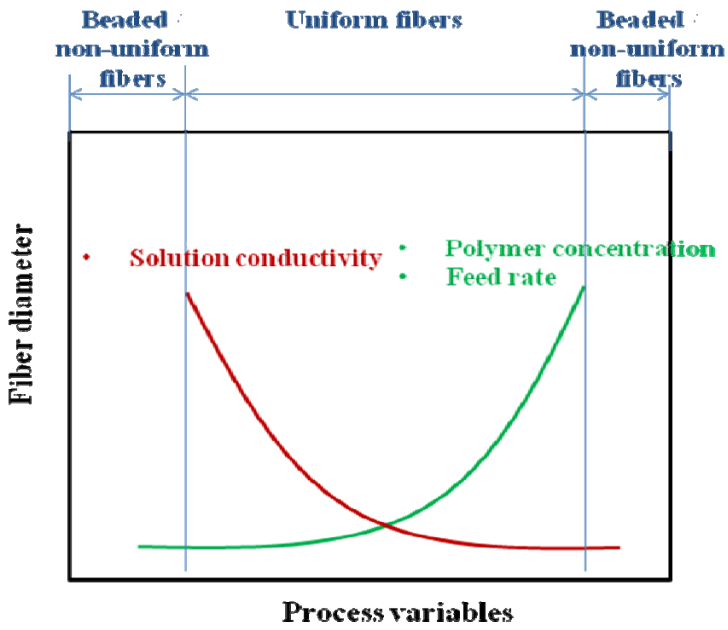

Figure 2.6. Processing map – Effect of process variables on fiber diameter [45]

2.5.3 Equipment variables

Most of the equipment variables affect the pattern in which the fibrous materials are collected (aligned, unaligned, tube-like or mat-like forms, etc.). There are a few equipment variables

that affect the fiber diameter; the needle (or nozzle) diameter is one of them. A larger diameter needle supplies a bigger droplet at the needle tip, resulting in larger jet radius and eventually larger fiber diameter [58]. Also, in such cases, multiple jets would be emanating from the needle tip, resulting in irregular fibers. Other equipment variables were already discussed section 2.3.

Ramakrishna et al. [45] studied the effect of various parameters (variables discussed above) and obtained a processing map in which the effects of important process variables are shown in Figure 2.6 [45]. This diagram gives us a general understanding of the major process variables and their effect on fiber diameter.

2.6 Scale up approaches

Electrospinning is a simple technique to fabricate nanofibers. However, fabrication rate of traditional needle electrospinning (TNE) is in the range of 0.01 – 0.1 g/hr [13] which has limited the industrial applications of electrospinning. The essential parameter in determining the fabrication rate from a single spinning site is the feed rate. However increasing the feed rate beyond a limit offers a large volume of fluid at the spinning site and this would require longer working distances (in order to solidify the jet) and higher electric field (in order to initiate jets at these longer working distances), limited by the electric breakdown strength of the spinning atmosphere (usually for air [61] ~3 x 10^6 V/m). In other words, increasing the feed rate as to the standards (~1 Kg/hr) of conventional fiber forming techniques would require a substantial increase in the velocity of the jets (probably up to speed of sound in air

[62]). Thus, a trade-off must be made between flow rate and field strength. Many researchers have attempted scale-up of the electrospinning process in more sophisticated ways, such as increasing the number of spinning sites. The previously reported approaches can be generally classified based on the feed method at the spinning site: either a confined or unconfined fluid-volume feed as shown in Figure 2.7.

2.6.1 Confined fluid flow

In confined feed systems, the polymer solution is injected at a constant rate (except for a few approaches which are gravity-assisted [64]) into an enclosed capillary (such as a needle or nozzle). High voltage is applied to the enclosure (or nozzle) or directly to the polymer solution using electrodes. Most scale up approaches based on confined feed systems utilize one or more [38, 63, 65-72] nozzles and each nozzle can produce one or more fluid jets, with additional jets formed by use of a grooved tip [12], a curved collector [65], or jet splitting [66]. Electroblown spinning [11] is another confined feed system similar to TNE electrospinning but using a controlled airflow near the lower end of the nozzle to aid in solvent evaporation and thus, allowing spinning at a higher flow rate than usual and an increased production rate.

Confined feed systems involving other enclosures continue to emerge and are well summarized by Zhou et al. [13]. These include the use of porous tubes with random and linear holes [73,74] conical wire coils with openings between the wires [64], multiple plastic tips where high voltage is applied directly to the polymer [48], a rotating cylindrical spinning

head with peripherally disposed extrusion tubes [75], a multi-channel microfluidic device [76], and electrospinning using charge injection [77]. In charge injection, when a net charge is injected to the fluid streams, it develops a self-electric field within the stream and stream surrounding it, thus causing breaking into multiple jets. The majority of scale-up approaches reported thus far utilize multiple nozzles with confined feed; hence, essentially, a linear scale-up of needle electrospinning. One of the major advantages of confined feed is the controlled flow rate, which is important for maintaining a continuous stable electrospinning process and controlling the nanofiber diameter (as higher flow rates are generally associated with thicker fibers). However, confined feed systems are innately prone to clogging, and require an engineered structure for each jet (or several jets), thus significantly increasing the complexity of the system [13].

2.6.2 Unconfined fluid flow

Conversely, in unconfined feed systems, a polymer solution flows over the surface of another material. Recent examples of such unconfined feed approaches include electrospinning from a polymer solution coating a metallic fluid in the presence of magnetic and electric fields (which results in spike-like structures) [78], the rotating cylindrical surface in the Nanospider^{TM} [79], cleft electrospinning [80], bubble electrospinning [81], and centrifugal electrospinning [82]. The Nanospider^{TM}, which is a commercially-available product, uses a rotating cylinder immersed in a polymer solution trough. In cleft electrospinning, jets are initiated using fine metallic points submerged under polymer solution and organize themselves to form a pattern on the free liquid surface. In bubble electrospinning, a gas-jet is

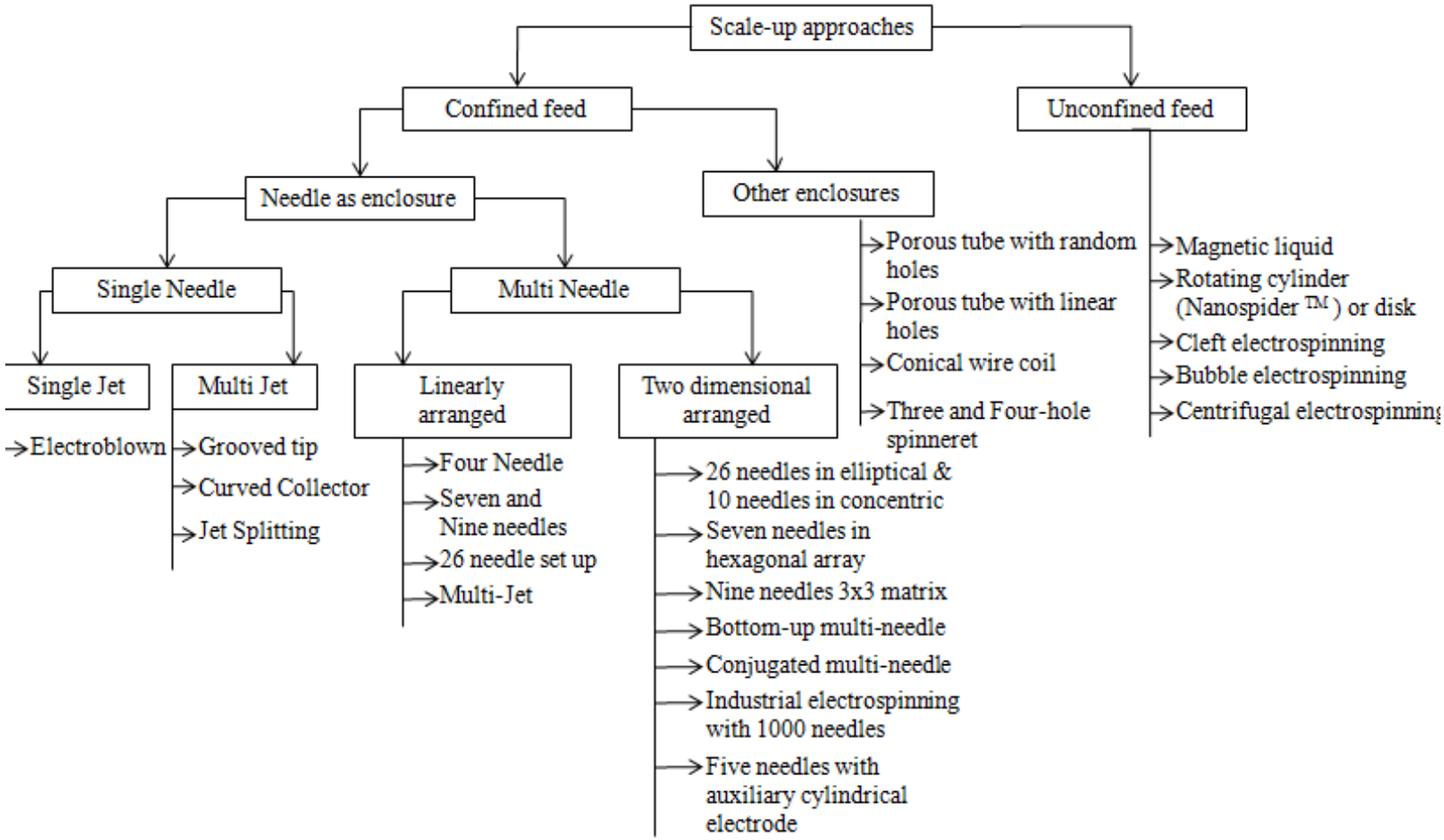

Figure 2.7 Classification of scale-up approaches

used to create bubbles in the polymer solution at which locations jets are formed. Finally, in centrifugal electrospinning, polymer droplets are fed onto a rotating disc and move radially to the rim of the rotating disc, where jetting occurs.

Challenges in unconfined feed systems are control of solution feeding, larger fiber diameter, and wider fiber diameter distribution. Because of the large number of potential jets, inter-jet interactions [48, 68] are a potential challenge for researchers exploring electrospinning scale-up.

2.7 Self-Assembled Monolayer (SAM)

This section introduces a technique -- growth of self-assembled monolayers -- utilized to modify the surface property of the source plate(s) which are used in this work. Self-assembled monolayers are single-molecule-thick collections formed by chemi- or physio-absorption onto a solid substrate [83-86]. In this work, silane precursor molecules are utilized which react with the hydroxyl groups on oxide surfaces and form chemical bonds to the surface (Figure 2.8). SAMs have widespread applications particularly to alter surface wetting properties, which is their main purpose in this work [87]. In this section, we discuss SAM formation technique and an application of SAMs related to the modification of surface wetting properties.

Figure 2.8 is a schematic describing the formation of a monolayer from decyltrichlorosilane onto a silicon-oxide terminated silicon surface. In this example process, the hydrophilic

silicon oxide is covered with a hydrophobic collection of alkyl chains. Hydrophobicity of a substrate can be measured by measuring the water contact angle. Figure 2.9 shows typical water contact angles of a substrate before, and after, SAM growth.

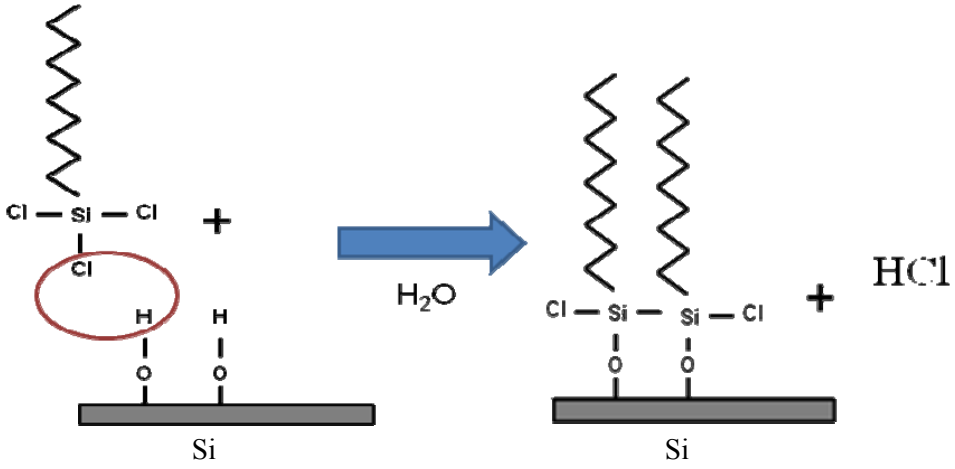

Figure 2.8 Formation of SAM on a silica surface using decyltrichlorosilane

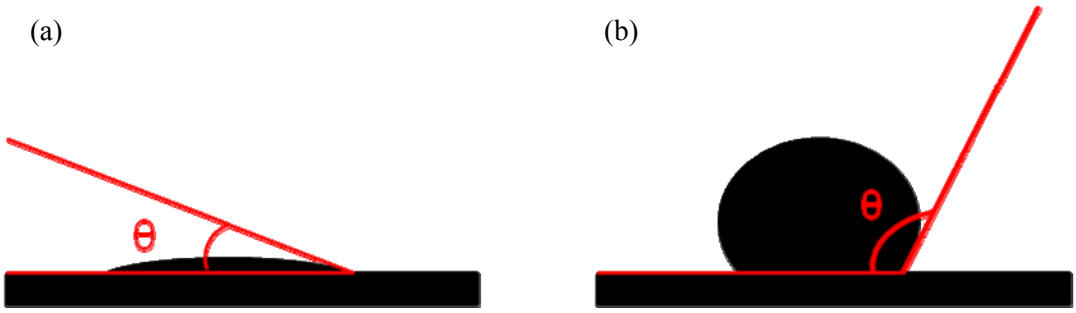

Figure 2.9 Representation of water contact angle (θ) of a substrate (a) before SAM and (b) after SAM

The water contact angle is the internal angle that a droplet makes when placed on a solid surface. Hydrophilic surfaces have small angles (<15º) whereas hydrophobic surfaces have larger values (up to ~120º).

In this work, SAMs are grown from the vapor phase, which provides a disordered surface film where the molecules are uniformly distributed [88]. This technique has been used in this investigation in order to modify the surface wetting properties of the substrate (aluminum with an oxide layer) to assist in electrospinning.

2.8 Electric field simulations

Characterization of the electric field magnitudes and spatial pattern is essential in understanding the electrospinning process. Differences in the geometric configuration of the electrospinning set up affect the electric field distribution. This section outlines a software Maxwell SV 2D that is used for analyzing electric field distribution of different geometries.

Each geometrical electrospinning configuration is considered as a *problem*. One or more two-dimensional slices are created and solved for each configuration. In defining the problem there are several steps; selecting the appropriate material for each component from the existing database (around 80 materials); setting up the boundary values/sources (to differentiate source and collector); setting up executive parameters (to indicate the signal and ground lines); setting up solution parameters; and finally solving the problem.

Maxwell SV 2D uses finite element analysis (FEA) to solve the problem through the following steps.

i) Automatically creates the required finite element mesh

ii) Iteratively calculates the desired electrostatic field solution until the solution converges.

iii) Provides the ability to analyze, manipulate, and display field solutions.

One can obtain different solutions/results at different mesh quantities. A converged solution (optimum or final solution) is obtained when the mesh quantity reaches maximum for the given problem. This maximum mesh size is found by the software through an iterative process. The user is allowed to choose number of iterations, or multiple cases with different mesh size, however once a converged solution is obtained, further iteration stops. “Post process” in the software allows plotting the solution as per users’ requirement.

Chapter 3

Research objectives

Electrospun nanofibers have widespread applications in tissue scaffolds, filtration, protective clothing, and optical electronics. However, the fabrication rate of the traditional needle electrospinning (TNE) process is very limited (on the order of 0.01 - 0.1 g/hr [13]). The scale-up approaches reported tend to be complex and/or can negatively alter the desired fiber morphology and quality. Thus, it is important to identify an approach to fabricate nanofibers with less complexity (still possessing the desired morphologies) and a high potential to scale-up for commercial viability. Towards this goal, obtaining fibers at truly the nanoscale (i.e. < 100 nm) with a narrow diameter distribution is equally important. This work focuses on an approach that shows promise for fabrication of electrospun fibers at the nanoscale from unconfined fluids, and the potential to significantly improve the fabrication rate. The research objectives are outlined below.

1. Investigate the prospect of electrospinning from a flat plate with unconfined fluids and further elucidate the fundamental physical process. This includes:
    a. Optimizing parameters such as polymer solution concentration, voltage, working distance and feed rate for a model system (poly (ethylene) oxide in water) via the traditional needle electrospinning (TNE) process. This will be used as a basis of comparison for this investigation.

b. Studying the electric field distributions of prospective geometries and identifying the fundamental requirements to initiate a jet from a proposed geometry.
c. Optimizing the parameters in the proposed geometry to fabricate electrospun nanofibers with morphological properties equal to or better than those in TNE and improved throughput.
d. Establishing processing parameter-fiber property relationships in the proposed geometry.

2. Analyze and compare the physical phenomena of the electrospinning process and the fiber/mat properties of the proposed geometry with respect to the TNE. This includes:
    a. Characterizing the jet profiles by imaging the electrospinning process in both the proposed and TNE geometries.
    b. Characterizing the morphology of nanofibers using scanning electron microscopy in both the proposed and TNE geometries.
    c. Evaluating the spinnability and porosity of nanofiber mats in both the proposed and TNE geometries.
3. Determining the scale-up possibilities of the proposed plate geometry. This includes:
    a. Evaluating the extent of scale-up possibilities with the proposed plate geometry.
    b. Applying the fundamentals of the current investigation to additional geometries.

Chapter 4

Experimental

4.1 Materials

Polyethylene oxide (PEO), with an average weight molecular weight of 400,000 g/mol (400k) (Scientific Polymer Products) was used without further purification. Solutions of 6 weight-percent (wt %) in de-ionized water, stirred for 24 hours at room temperature to aid dissolution, were used for all experiments. Rhodamine 590 chloride (R6G) (Exciton) was used (0.001 wt %) to enhance imaging contrast when viewing the electrospinning process (especially Taylor cone). Viscosity measurements were done using Stresstech instruments RHEOLOGICA Instruments AB at 25º C and zero-shear viscosity was found to be 9250 cP. Polycaprolactone (PCL), with a number average molecular weight of 70,000 – 90,000 (by GPC) (Scientific Polymer Products) was used without further purification. Solutions of 12 weight-percent (wt %) in dimethyformamide (DMF) and dichloromethane (DCM) (solvent ratio 1:1), stirred for three hours at room temperature were used at particular instances which are further discussed in results section.

The source plates were treated with silanes containing a hydrophobic terminal group (decyltrichlorosilane (C_{10})) (Sigma Aldrich), which formed alkylsiloxane self-assembled monolayers on the plate surface (SAMs), in order to decrease interactions between the water-based polymer solution and the plate. The aluminum source plates (4" x 1½" x 1/16" (length x width x thickness)) (McMaster Carr) were cleaned in a UV-ozone cleaner for 30 minutes

(10 minutes with oxygen) to enhance the number of available hydroxyl groups for the film growth reaction and ensure suitable surface cleanliness. These plates are further referred as *A type* plates. The plates were preheated in an oven for 30 minutes at 90° C then exposed to C_{10} vapor for 1 hour. During this process, the hydrophilic hydroxyl surface groups react with, and are covered by, the alkyltrichlorosilanes, which ultimately form a disordered monolayer with a hydrophobic methyl and methylene-terminated surface [85]. Plates were rinsed with methanol for 10 seconds and sonicated in toluene for 10 minutes to remove any material not permanently attached to the surface. This process provides a disordered but hydrophobic monolayer-like coating of the metal plate surface. Water contact angle (droplet size 2 μl, average of five readings) on aluminum plate before film growth was ~ 0º (i.e., the water wetted the surface), and after treatment was 105 ± 3º (Figure 4.1a). For the PEO:water

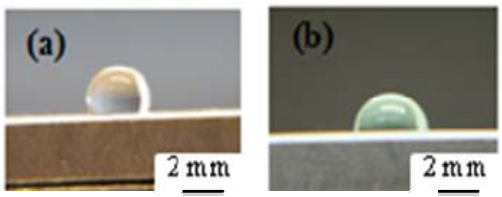

Figure 4.1 Contact angles measurements for an aluminum plate whose wettability has been chemically modified by treatment with decyltrichlorosilane (C_{10}) for (a) water (105 ± 3º) and (b) 6 wt % PEO+water spinning solution (87 ± 3º).

solution used for electrospinning, the contact angle on the hydrophobic coating was 87 ± 3º (Figure 4.1b). Aluminum collector plates (15" x 12" x 1/8") (McMaster Carr) were used without further treatment. In preliminary experiments, for a flat plate configuration two

identical plates (12" x 8" x ¼") made of aluminum (McMaster Carr) were used and one of them was treated with C_{10} in order to obtain a hydrophobic surface. These plates are referred as *B type* plates.

4. 2 Apparatus

A commercial power supply (Glassman High Voltage Model No. FC60R2) provided positive polarity, high voltage to the source plate (or needle), while the collector plate was held at ground potential. Aluminum foil covered the collector plate in order to gather the electrospun mat samples for further measurements.

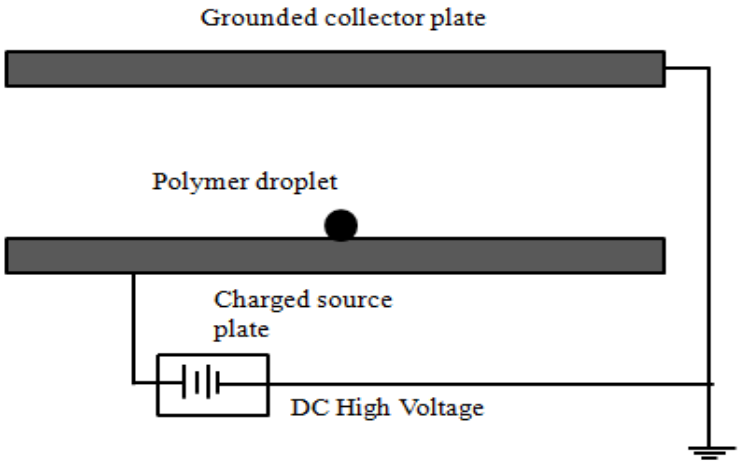

Figure 4.2 Flat plate configuration with a polymer droplet at the center of the plate

For quantitative analysis of the linear and whipping regions of the electrospinning process, a camcorder (Panasonic SDR – H60) (with a 6 mm x 18 mm T monocular (Zeiss) to capture

Taylor cone) recorded images while the polymer jets were illuminated with industrial video lighting equipment (Olympus).

Figure 4.2 shows an initial set up where two identical plates (B type) were placed horizontally separated by certain distance. The source plate treated with C_{10} was placed at the bottom and connected to power supply while the collector was placed at top and grounded.

Two other configurations (in addition to TNE) (which are the principle investigation apparatus) were utilized for electrospinning as shown in Figure 4.3a and 4.3b.

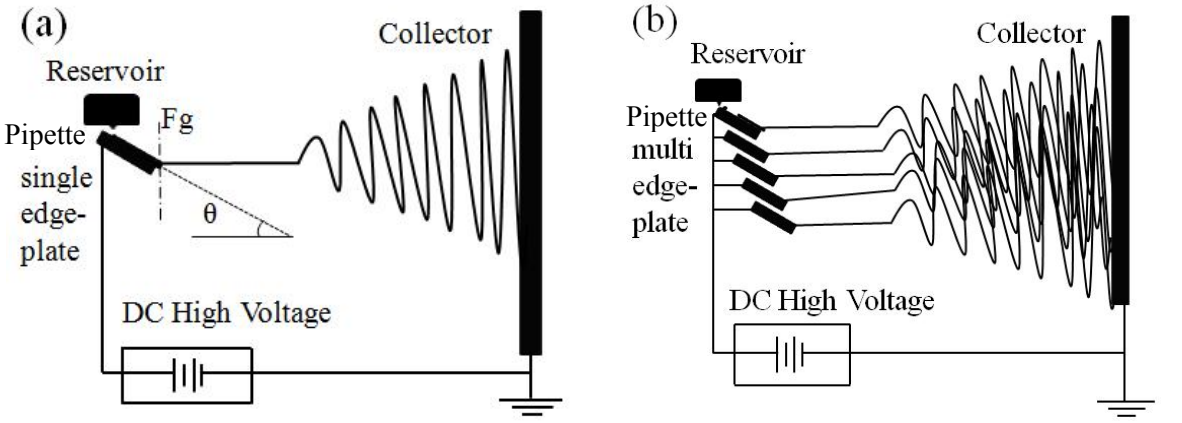

Figure 4.3 (a) Illustration of single edge-plate electrospinning, θ and direction of gravity (F_g), and (b) Multi-plate electrospinning ("waterfall")

The edge-plate configuration consisted of an aluminum source plate (A type) held at 40º (θ) to horizontal with a vertical collector plate, as mentioned in previous section and as indicated in Figure 4.3a. Additionally, multiple thin plates (A type) were stacked to form a *waterfall* spinning configuration (Figure 4.3b) with collector. Each plate was attached to the high voltage power supply. In either configuration, an electrically insulated reservoir fitted with

one or more plastic pipettes supplied polymer solution to the charged plate. For the solution viscosity used here (9250 cP), the solution traveled in a straight line from the pipette down the plate with little branching. All plates were treated with the C_{10} monolayer as described above. The working distance refers to the distance between the edge of the source plate (bottommost plate in case of waterfall configuration) to the grounded collector plate surface.

Polymer flow was gravity-assisted and thus dependent on the angle at which the plates were held, the volume of the solution in the reservoir, and the pipette aperture size. For a successful continuous electrospinning process, the polymer flow rate should be balanced by the polymer loss caused by the jet formation. The presence of excessive fluid volume in the jet initiation region was associated (in the presence of high electric fields) with electrospraying or streaming (discussed in detail in section 4.2) events. In order to determine the optimal polymer flow, survey experiments were carried out at different plate angles from 20º to 70º and most favorable results were obtained at 40º; this angle was subsequently kept constant throughout the study. For flatter plate orientation (lower angle), the supply of solution was insufficient to maintain a continuous jet. At steeper plate orientation, excessive volume would drip from the plate frequently (occasionally streaming). In all experiments, a 50 ml solution was placed in the reservoir with a pipette inner diameter of 1.5 mm. In most of the electrospinning experiments, a maximum of 3 ml out of the total volume was utilized. At these conditions and with a polymer solution zero-shear viscosity of 9250 cP, the flow rate was found to be approximately 30 µl/min. Flow rates were varied using different pipette sizes (2.0 mm diameter for 45 µl/min and 2.3 mm diameter for 55 µl/min).

4.3 Fiber characterization

Nanofiber morphology was studied with a Phenom SEM (FEI) operating at 5.0 kV. The samples were coated on a S67620 mini sputter coater (Quoron technologies) with Au-Pd at a thickness of 100 Å to reduce charging and produce a conductive surface. The SEM images were analyzed using ImageJ Analyzer software to determine diameter and porosity characteristics; 25 individual measurements made on each sample determined the mean nanofiber diameter and standard deviation.

Porosity is measured using ImageJ Analyzer software by converting SEM images into grey scale where the fibrous area is differentiated from voids. Porosity values are determined as a percent of void area to the total area of the mat. In this analysis, a single layer of the fibrous mat is considered for all samples.

Spinnability is defined as the measure of percent of dry fibrous area to the total area of the fibrous mat. Undried areas are visible and appear like patchy lines on the images of fibrous mat. These portions are marked in different color using MS-paint software and then converted into grey scale using ImageJ analyzer in order to find the percent of the dried fibrous area to the total area of the mat.

4. 4 Electric field simulations

Electric field distributions for different electrospinning geometries (TNE, parallel plate and edge-plate) were modeled using Maxwell SV 2D (2 dimensional) software. The mesh size

was increased until the solution converged. Although a two dimensional analysis of a three dimensional structures has limitations, by considering the symmetry of the arrangements in question, the two dimensional calculation can be viewed as a planar slice through the three dimensional apparatus and, therefore, captures the most relevant physical parameters of the design. Electric field simulations were modeled for each geometry as specified in section 4.2 with different configurations (working distance and applied voltage) and discussed in following chapter. For TNE geometry, the source plate (Figure 4.3a) is replaced with a stainless steel needle of size 4" in length and 0.9 mm in diameter.

Chapter 5

Results and discussion

5. 1 Electric field simulations

Electric field strength and homogeneity in various electrospinning configurations (using Maxwell SV 2D software as described above) is discussed. Qualitatively, the TNE geometry results in a very inhomogeneous field with the strongest field and field gradient at the needle. Conversely, pure parallel plate geometry (identical plates that are placed horizontally one above the other separated by a certain distance, Figure 4.2) results in a homogeneous field (i.e., no field gradient) at the center of the plates and a lower maximum field compared with TNE. However, within the parallel plate geometry, the sharp edges of the plate can still result in a strong electric field and field gradient at those locations. One could then imagine easily forming many spinning sites along the entire edge; a more facile approach to parallel spinning sites than employing an array of needles. It is observed that since the strongest electric field and the strongest gradient tend to occur at the same location, one goal of this work is to decouple the two effects. As discussed later, the electric field gradient at the location of jet formation appears to be the most important parameter to ensure effective fiber formation. It is important to note that while the electric field can be increased by simply increasing the voltage, the electric field gradient is geometry-specific.

These observations can be quantified and shown in Figures 5.1 – 5.3 with magnitude E [V/m] and the small box inside the image shows the magnification of the tip of the source.

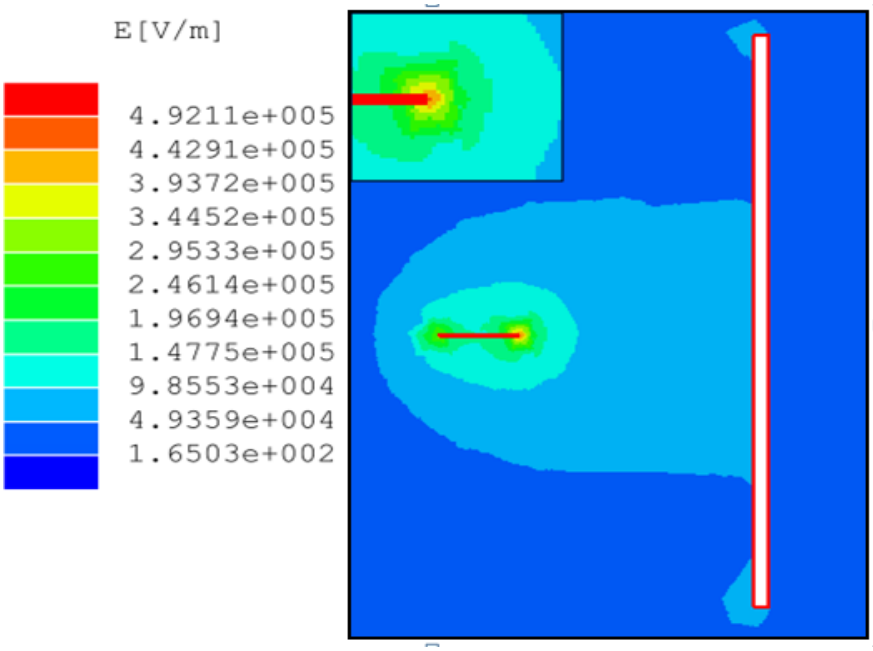

Figure 5.1 Electric field distributions for TNE geometry with 15 cm working distance and 15 kV

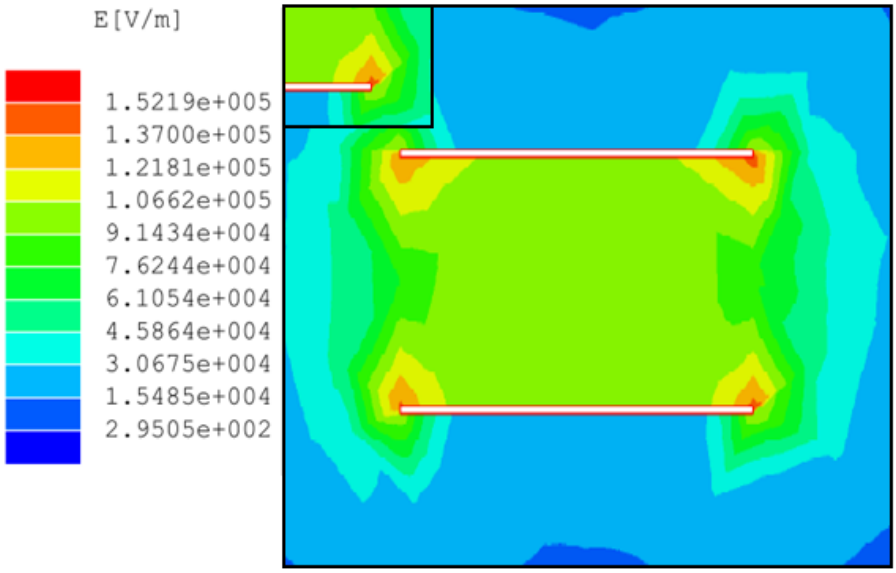

Figure 5.2 Electric field distributions for parallel plate geometry with 15 cm working distance and 15 kV

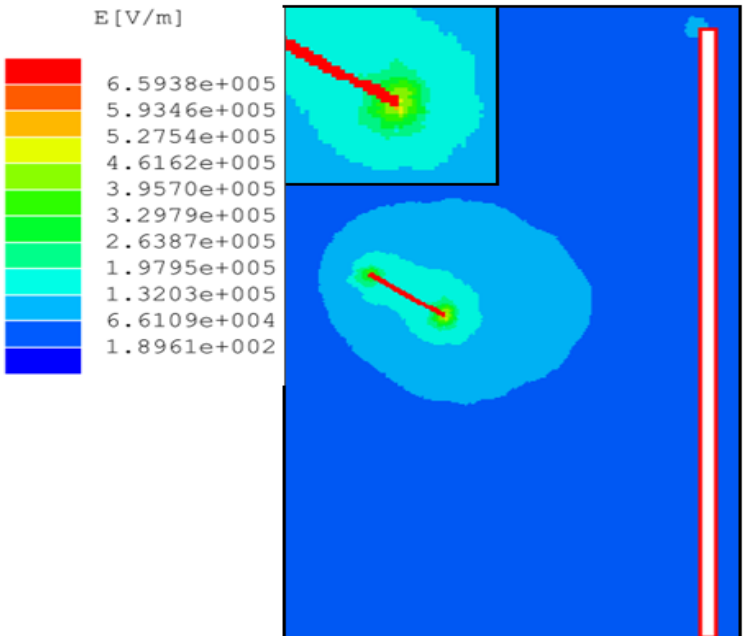

Figure 5.3 Electric field distributions for edge-plate geometry with 15 cm working distance and 15 kV

For an applied voltage of 15 kV and 15 cm working distance, in the TNE geometry (Figure 5.1), the magnitude of the simulated electric field (E) near the needle tip is $4.2 \pm 0.2 \times 10^5$ V/m and gradually decreases to $7.5 \pm 2.5 \times 10^4$ V/m at the collector. Applying the same voltage and working distance in the parallel plate geometry (Figure 5.2), at the center of the source plate $E = 1.0 \pm 0.2 \times 10^5$ V/m and does not vary significantly from that point to the collector (resulting in no electric field gradient). Thus, in comparison, the TNE configuration has a higher field magnitude and a larger field gradient. However, the electric field at the source plate edge ($1.3 \pm 0.1 \times 10^5$ V/m) (in the parallel-plate set up) is higher than between the plate centers and results in a non-zero electric field gradient. These simulated electric field distributions correspond with other reports of the TNE geometry and of unconfined feed electrospinning using cylindrical and disk spinning sources [64, 89]. In

particular, the effect of higher field strength at the plate edges could be compared to the cylindrical nozzle edges which displayed a higher magnitude electric field than that at the center of the cylinder.

The higher electric field exhibited at the plate edge can thus be utilized more efficiently in the edge-plate geometry (Figure 5.3). In the edge-plate geometry, for the same voltage and working distance, the maximum field is quite similar to that in the TNE configuration in magnitude and gradient, that is $4.3 \pm 0.3 \times 10^5$ V/m at the edge and gradually decreasing to $7.5 \pm 2.3 \times 10^4$ V/m at the collector. This indicates that the edge-plate geometry could be a direct substitute for TNE but with many more potential spinning sites. However, even though the electric field parameters are similar, in the edge-plate scenario, an unconfined flow of polymer solution over the surface of the plate might alter the stability, effective flow rate, and size and shape of the linear and whipping regions during spinning and thus the resultant nanofiber quality, such as the average fiber diameter and diameter distribution. The results discussed below that indicate these factors can be overcome and that nanofibers spun from the same solution in TNE and edge-plate configurations have very similar diameter distribution and average size. However, higher mass throughput is obtained when utilizing the edge-plate configuration.

5.2 Jet formation

Parallel-plate configuration was utilized for our initial experiments to study jet formation. Unless otherwise noted, a PEO polymer solution of a concentration suitable for TNE was

utilized (see experimental section above). Use of the same solution enabled direct comparison between fibers generated by TNE and other configurations. In the parallel-plate configuration two identical horizontal plates are used with the source plate placed at bottom and the collector plate at the top, separated by varying fixed distances. In this scheme, different size droplets were placed at the center of the source plate and a range of electric fields were applied. Application of very high electric fields (40 kV for a 10 cm working distance) did not result in jet formation at locations near or at the center of the plate. At this voltage, the electric field at the center ($4.0 \pm 0.2 \times 10^5$ V/m from simulations) is similar to that in standard TNE configuration (11 kV and 15 cm working distance). However, the electric field gradient is essentially zero, in contrast with TNE. When droplets were placed near the plate edges, the droplet deformed, jetting occurred, and electrospraying was observed above 30 kV applied voltage (effective electric field $4.5 \pm 0.2 \times 10^5$ V/m). (This electrospraying could be due to the fact that the short working distance required to obtain the high electric fields did not provide a suitable distance for the water in the PEO solution to evaporate, and therefore resulted in *jet streaming* (a jet that does not whip and hits the collector before the solvent is completely evaporated).) Under the same processing conditions with a non-treated plate, we utilized a lower viscosity solution (polycaprolactone (PCL) solution in a more volatile solvent system (chloroform and dimethyl-formamide). Again, no jet formation occurred for droplets placed near the center of the source plate, for average electric field up to 4.0×10^5 V/m (average electric field is applied electric field divided by the working distance). However, electrospinning and fiber formation was observed for droplets placed near the edges of the plate with an applied voltage of 25 kV at a

10 cm working distance (2.5 x 10^5 V/m). Even when the electric field at the plate center was tuned (by increasing the applied voltage) so that it was the same magnitude as that for successful spinning from the edges, no jetting was observed from the plate center. To summarize, in regions where the electric field is highly homogeneous no jet formation was observed, for a wide range of applied electric fields and two different viscosity solutions. On the other hand, jet formation was seen for both solution types near the plate edges. Therefore, the electric field inhomogeneity (i.e., a field gradient) in these regions favors jet formation, as also discussed by Yang et al. [28].

With edge-plate configuration, (similar to Figure 4.3a), but the plate is held flat ($\theta = 0^o$), the results were similar as mentioned in parallel plate, where high electric field strength was required to initiate jetting from drops, however resulting in jet streaming. In further investigations with the edge-plate configuration, the plate was fixed at an angle as shown in Figure 4.3a. PEO solution was fed by gravity from a reservoir at the top of the plate. Near the lowest edge of the plate, and in particular, where the polymer solution thinned and became a pendent droplet hanging from the plate edge, electrospinning was observed. This result is likely the combination of the electric field gradient at the plate edge and the changing geometry of the hanging fluid. The sequence of jet formation is shown in Figure 5.4. For better imaging contrast, the PEO-polymer solution is tinted with 0.001 wt% R6G. As the polymer solution reaches the edge of the surface treated plate (Figure 5.4a.) the viscoelasticity of the solution maintains the shape (does not drip or fall off immediately), even past the plate edge (Figure 5.4b.). However, eventually a neck forms between the fluid

on and off the plate (Figure 5.4c.) and the pendent droplet elongates. The simultaneous elongation of the fluid (Figure 5.4d.) and presence of the strong electric field and electric field gradient at the plate edge couple to create jet initiation (Figure 5.4e.). The jet from the Taylor cone forms a linear region followed by a whipping region in analogy to the TNE process.

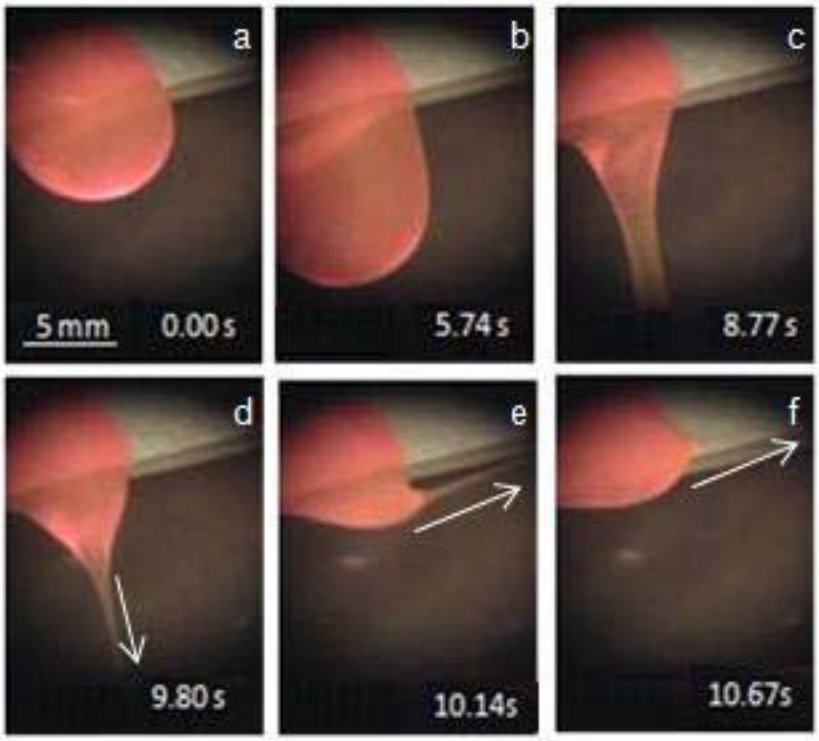

Figure 5.4 PEO-polymer solution droplet (doped with R6G) falling from the plate, and the subsequent jet initiation process. Sequential video images taken under room light illumination. Arrows in the images (d, e and f) shows the jet direction.

A minimum electric field magnitude for a working distance of 35 cm at the edge (as estimated from the simulations) of $4.60 \pm 0.2 \times 10^5$ V/m was required to initiate the jets. (The magnitude of this electric field is similar to that used in the parallel-plate measurements,

however, in those experiments, no jet formation was observed.) The successful jetting process here is a result of the combined effect of the thinning of the polymer solution due to gravity and the field gradient at the plate edge. In a recent work [89] on needleless electrospinning (using a rotating cylinder (that provides a lesser gradient at the cylinder edges)) with polyvinyl alcohol (9.0 wt % in distilled water) solutions of 1620 cP viscosity, for stable electrospinning, an electric field of $5.8 \pm 0.4 \times 10^5$ V/m (computed using the reported spinning parameters for Maxwell SV 2D simulations. In contrast, in the PEO experiments reported here with a significantly higher viscosity (9250 cP) solution, the minimum electric field at the jet location is slightly less and comparable to TNE which is $4.6 \pm 0.2 \times 10^5$ V/m for 35 cm working distance. Thus edge-plate geometry provides a sharp electric field gradient at the edge that assists in the initiation of jets at electric potentials similar to TNE process. In addition, thinning of the polymer solution by gravity also assists in jet initiation.

In the edge-plate geometry, it is interesting to observe that the Taylor cone is formed on the free surface of the polymer solution (Figure 5.4f.). Thus, as the fluid flows, the Taylor cone moves dynamically, mostly forming in the narrowest fluid region and the strongest electric field/field gradient region near the edge of the plate. Such locations are referred as *spinning sites*. In order to obtain a stable electrospinning process, there should be optimum supply of polymer solution to the spinning site. In the edge-plate configuration, the polymer flow is partially controlled by the angle at which the source plate is held (θ as shown in Figure 4.3a). For the given viscosity and spinning parameters, an optimum supply of polymer solution is

observed when θ = 40º (as discussed above), above which there was an excessive supply that caused frequent drip off and below which the jet was depleted of polymer solution. Both solution scarcity and excess resulted in extinction and re-creation of the jet, and thus an intermittent rather than continuous electrospinning process.

5.3 Jet profiles

Jet profiles for TNE and edge-plate electrospinning were compared; Table 5.1 summarizes the length of the linear region, cone angle (full cone angle) of the whipping region and the diameter of the resultant mat on the collector. Also for each configuration, the electric field at the tip of the source (needle or edge) and near the collector is specified to develop an understanding of electric field distribution while studying the jet profiles. Discussion in this section is focused on the linear region, the whipping region and the factors affecting each.

Table 5.1 Electric field strength and jet profiles measurements of TNE and edge-plate electrospinning process.

Set up	Working distance (cm)	Field Strength E [V/m]		Linear region		Whipping angle (Full cone angle)		Average deposition on collector (diameter in cm)
		at Tip of the source	near the collector	Length (cm)	Percentage of working distance	Primary (°)	Secondary (°)	
TNE	15	$3.0 \pm 0.2 \times 10^5$	$9.2 \pm 1.5 \times 10^5$	3.3	22.00%	48.6	-	6.5
TNE	35	$4.8 \pm 0.3 \times 10^5$	6.5×10^4 - 5.1×10^2	8.3	23.70%	26.3	47	14
Edge-plate	35	$4.6 \pm 0.3 \times 10^5$	6.2×10^4 - 3.9×10^2	9.9	28.20%	34	60.5	18

As shown in Table 5.1, for a normal working configuration, needle electrospinning has a small linear region which represents ~22% of the total working distance. In TNE, the linear region length, L, is given by Equation 4 [40,43] (as discussed in section 2.4.2) where K is the solution conductivity, Q is the feed rate, ρ is solution density, χ is the aspect ratio of jet, E_α is local electric field strength, I is electric current and έ is the dielectric constant. In TNE, the size of the linear region with different feed rates (5, 7.5, 10 and 12.5 µl/min) keeping the electric field and working distance constant were studied. These results also show that increasing feed rate increases the linear region. Subsequently, this reduces the length of the

$$L^5 = \frac{K^4 Q^7 \rho^3 (\ln\chi^2)}{8\pi^2 E_\alpha I^5 (\acute{\varepsilon})^2} \qquad (4)$$

whipping region and so the jet spends less time in whipping, resulting in larger nanofiber diameters. In Figure 5.5a, the effect of feed rate on length of the linear region (in % of the total working distance, left ordinate) and fiber diameter (right ordinate) and are presented. In TNE, it is observed that fiber diameter increased as the feed rate was increased up to 12.5 µl/min. (At feed rates greater than this, solvent evaporation is not complete and residual solvent is deposited on the collector.) In edge-plate geometry, the linear region is longer, approximately 28% of the total working distance (Table 1). The increase in the linear region is due to the higher flow; a similar trend is seen in TNE under similar conditions (voltage (28 kV) and working distance (35 cm) with a larger needle diameter-to accommodate greater fluid volume) as a function of feed rate, as shown in Figure 5.5b. There are two important observations from this comparison. First, there is no statistical difference (within the

standard deviation) for the length of the linear region and the average fiber diameter between the two methods; second, for TNE, there is a discontinuous change (drop) in the fiber diameter as the spinning parameters are changed to accommodate the higher feed rates.

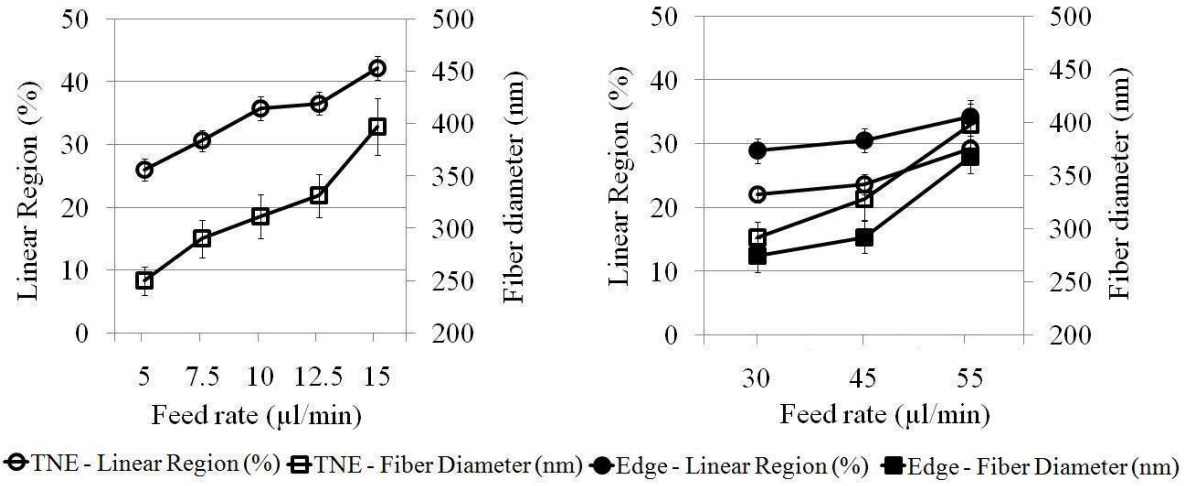

Figure 5.5 (a) Average fiber diameter and jet linear region length vs. feed rate in (a) TNE process with 15 cm working distance and 11 kV (b) TNE and Edge plate electrospinning process with 35 cm working distance and 28 kV.

Whipping cone angles for both geometries are summarized in Table 5.1. Whipping cone angles are measured by analyzing the images (jet profile images/snapshots obtained videos taken using camcorder during electrospinning) in ImageJ analyzer. In edge-plate electrospinning, an extended whipping region (secondary cone) at higher working distances was observed which was quantified by measurement of a secondary full cone angle. When longer working distances were evaluated for TNE, this secondary cone was also seen. Figure 5.6 shows a schematic representation and a photographic image (Figure 5.6b) of the full cone angles where the secondary cone appears a certain distance after the primary cone.

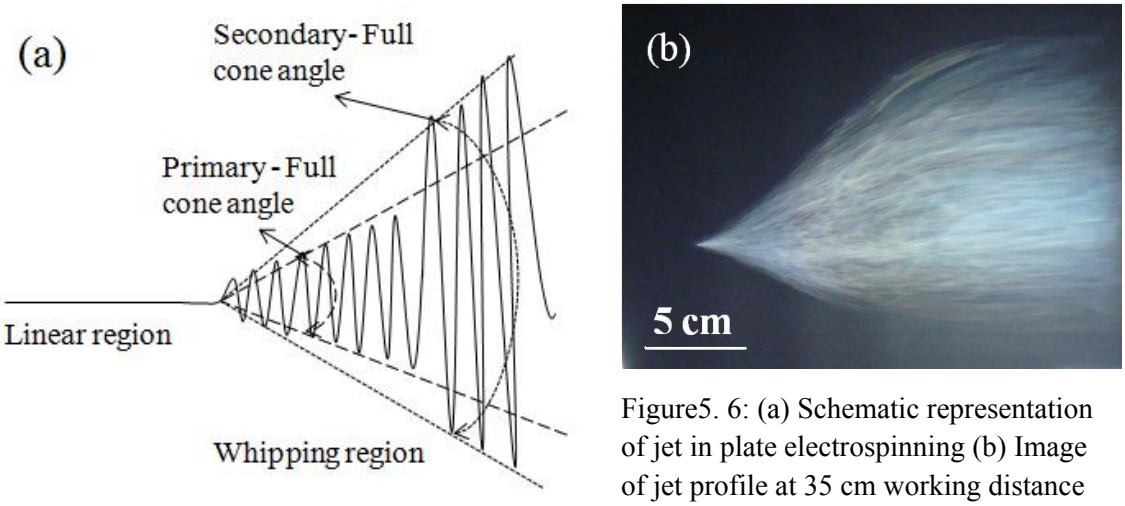

Figure5. 6: (a) Schematic representation of jet in plate electrospinning (b) Image of jet profile at 35 cm working distance

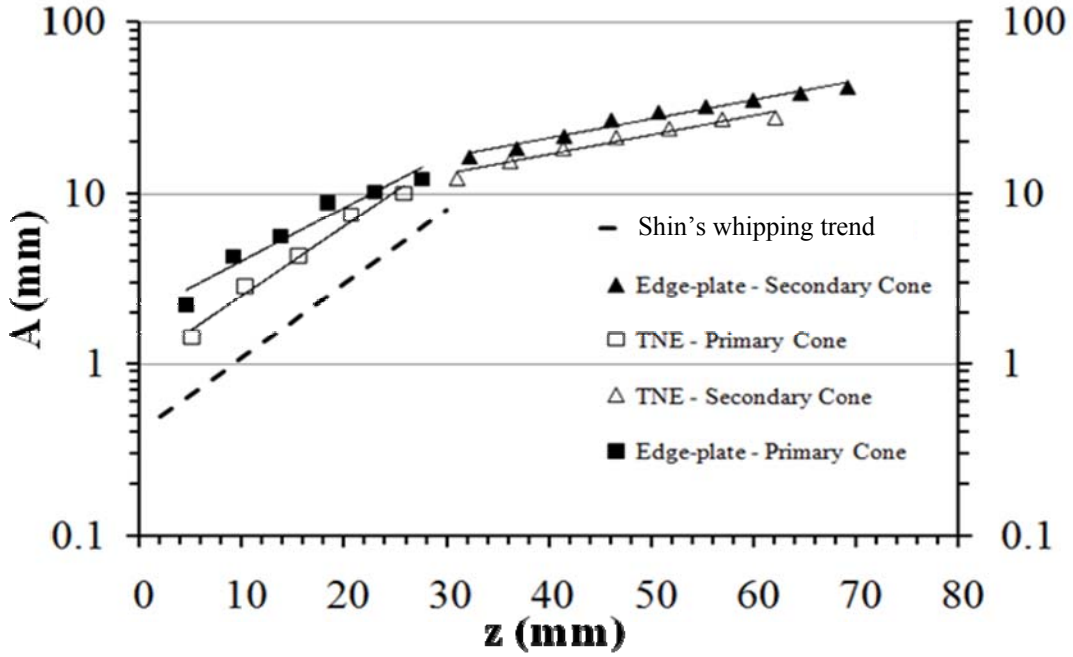

Figure 5.7: Amplitude A of whipping instability as measured from the radius of the instability envelope vs. axial distance (z) from the onset of whipping instability fit to an exponential function. Shin's whipping trend is shown with a dotted line in conjunction with the primary and secondary cones observed in TNE and edge-plate electrospinning for this work.

It is germane to note that the secondary cone is only seen at working distances of 35 cm or greater (for both TNE and edge-plate). Shin et al. [90] quantified the cone envelope as a function of distance from the onset of the cone and found it fit an exponential function. Figure 5.7 shows the Shin data (for PEO and water (where only a primary cone angle was observed)) along with our TNE and edge-plate configurations. Here, the cone envelope for the secondary cone is also plotted, which is also exponential, but fits with different coefficients than the primary cone (i.e. it is discontinuous). Therefore, it is clear that the secondary cone is a unique feature for longer working distance electrospinning (for both TNE and edge-plate). This secondary cone might be associated with subsequent cycles of bending instabilities (as discussed by Reneker et al.) [42], and therefore, is more easily observed at longer working distances. This hypothesis supports the above observation (Figure 5b) that at working distances above 35 cm (where the secondary cone is visible and hence more whipping takes place) the fiber diameter drops below that for working distances less than 35 cm.

5.4 Processing parameters-fiber properties relationships

5.4.1 Fiber diameter and diameter distribution

5.4.1.1 Effect of fluid flow

Figure 5.8 shows SEM image of PEO electrospun nanofibers obtained from TNE and edge-plate geometry. Fibers obtained from TNE with process parameters 15 cm working distance, 11 kV (average electric field 7.3 x 10^4 V/m), at a feed rate of 5 µl/min resulted in fiber diameters 243 ± 19.2 nm. For the same solution, with 35 cm working distance, 28 kV (8.1 x

10^4 V/m) and a feed rate of 30 µl/min, edge-plate electrospinning resulted 275 ± 32 nm. The mean diameter of the edge-plate electrospun fibers is approximately 10% bigger and the standard deviation is larger than that for the optimized TNE process. The increase in the fiber diameter is likely due to the higher feed rate. As discussed in section 5.3, higher feed rates increase the linear region which decreases the whipping region and results in a larger fiber diameter. When edge-plate is compared to TNE under similar conditions (35 cm working distance, 28 kV and 30 µl/min) the resulting TNE nanofibers have an average diameter of 292 ± 28 nm, which is slightly larger but overlaps with that for the edge-plate electrospun fibers. Thus, we conclude that the primary reason for the increase in the average fiber diameter typically reported for unconfined systems is due to the increased feed rate.

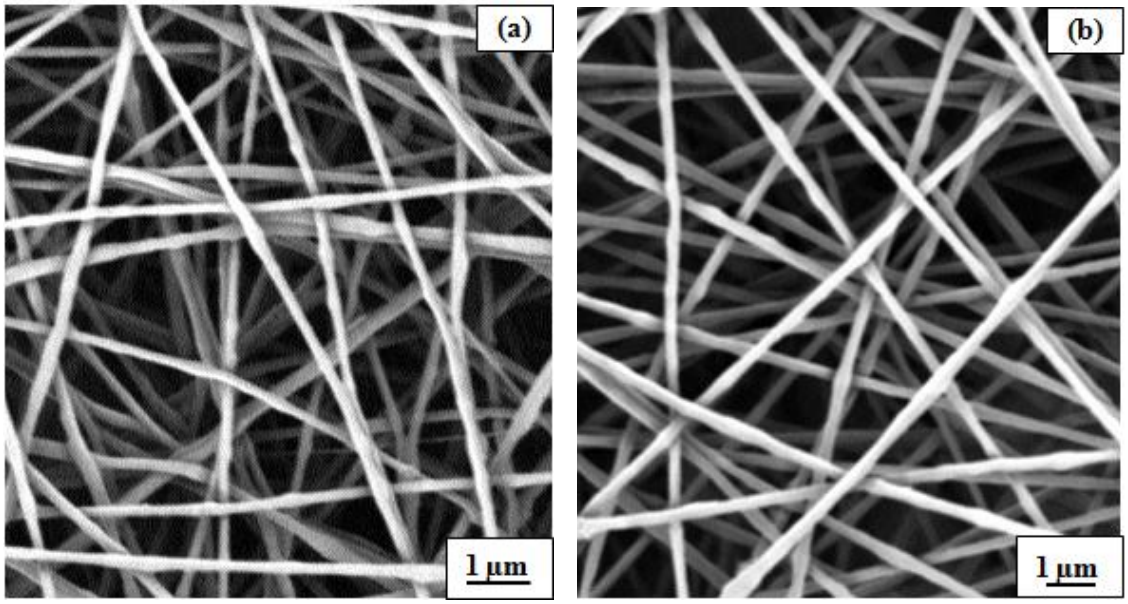

Figure 5.8: Comparison of electrospun nanofibers from (a) TNE geometry at 15 cm working distance and 11 kV (b) edge-plate geometry at 35 cm working distance and 28 kV.

In previous work [78, 89, and 91] where PEO and other polymer nanofibers were electrospun using different unconfined geometries, fiber diameters were found in the range between 200 - 800 nm with very large standard deviations. It was reported [89] that larger fiber distribution using a cylindrical nozzle was due to the difference in the electric field magnitude at the edges and center of the cylinder which produced finer and coarser fibers respectively. Another reason for larger fiber diameter and distribution could be the unconfined fluid flow rate (and resulting volume accumulation). In most of the unconfined geometries, the fluid flow at the spinning site is seldom controlled. In edge-plate geometry, these issues were overcome. The electric field magnitude and gradient is constant at the spinning sites (the plate edge); and the fluid flow to the spinning site can be controlled by fluid viscosity, pipette diameter, and plate angle. Thus it is facile to tailor the edge-plate parameters to achieve fiber diameters and diameter that are similar to TNE process.

5.4.1.2 Effect of applied voltage and working distance

Applied voltage and working distance did not have a significant effect on the fiber diameter. In this study with edge-plate geometry, three working distances (25 cm, 35 cm and 45 cm) and three average electric field strengths (9.1×10^4 V/m, 1.0×10^5 V/m and 1.1×10^5 V/m) were utilized. Fiber diameters showed a slight trend upward with increased applied electric field, and a trend of decreasing diameter with increased working distance. However these trends were smaller than the standard deviation of the diameter distribution, ~30 nm. Previous work in TNE and in needleless electrospinning [89, 91] also reported that the fiber

diameter of electrospun materials was not significantly affected by applied electric field, consistent with the results from edge-plate spinning.

5.4.2 Spinnability and Porosity

In TNE, at very high feed rates (more than 12.5 µl/min at 15 cm working distance and 11 kV, as discussed in section 4.3) solvent evaporation is not complete and the residual solvent deposits on the collector.

In both TNE (up to a 12.5 µl/min feed rate with 15 cm working distance and 11kV) and single edge-plate electrospinning (up to a 45 µl/min feed rate with working distance 35 cm and 28 kV), spinnability values were 100%. However, at a 55 µl/min feed rate, solvent evaporation during jetting was not complete; in addition, the higher throughput caused intermittent spinning that resulted in streaming (discussed in 4.5.2) and spinnability was found to be 98.5%. Also shorter working distances (25 cm) in edge-plate geometry (at different feed rates) did not allow for sufficient solvent evaporation, resulting in an average spinnability of 97.0%.

The porosity of TNE electrospun mats studied here were 64.5 % (±3.0) (working distance 15 cm and an average electric field of 7.3 x 10^4 V/m) and edge-plate electrospun mats exhibited higher values like 70.1 % ± 4.2, 71.2 % ± 4.8 and 74.2 % ± 4.7% for working distances 25, 35 and 45 cm, respectively (average electric field of 8.1 x 10^4 V/m). This difference is attributed to the shorter working distance (TNE) between the needle and the collector plate:

the longer the working distance, the higher the porosity. This was confirmed with the TNE fibers electrospun at longer working distance (35 cm) at same average electric field which was 70.0 % ± 3.0%. Also it is evident from the previous discussion that increased working distance increases the whipping cone angle and this eventually gives a well spread collection on the grounded collector. Hence, the overall porosity of the nanofibrous mats increases as the working distance increases.

5.4.3 Effect of multiple feed streams on morphology and production rate

Up until this point, spinning has occurred from a single source (i.e,. a single pipette creating one fluid stream). Here, the effect of several pipettes, and therefore multiple fluid streams on the fiber morphology and production rate are discussed. Table 5.2 summarizes the set of

Table 5.2: Effect of multiple spinning sites (pipettes) on average fiber diameter and fabrication rate

Number of pipettes	Center to center distance between pipettes (cm)	Average fiber diameter (nm)	Fabrication rate (gm/hr)
1	-	275 ± 32	0.13
2	4.8	278 ± 28	0.24
3	2.4	290 ± 41	0.27
5	1.2	311 ± 54	0.19

experiments that were done with 35 cm working distance, 28 kV and 30 µl/min (using a pipette size of 1.5 mm). Uniform electric field magnitude and gradient is ensured at all

spinning sites by having the fluid stream away from the corners of the plate (corners of the plate have higher electric field magnitude and gradient).

Fabrication rate in each case was calculated by a 20 minute test experiment. In order to compare with the TNE process, a similar 20 minute test experiment was conducted in TNE with 15 cm working distance, 11 kV and 5 μl/min (standard working condition) that resulted average nanofiber diameter of 243 ± 19.2 nm with a fabrication rate of .027 gm/hr (Fabrication rates for TNE are typically in the range of 0.01 – 0.1 g/hr [74]). From Table 2, it can be noted that fabrication rate of edge-plate (with a single pipette) is approximately 10 times higher than TNE. Increasing the pipette quantity increased the fabrication rate. However when employing three pipettes (three spinning sites) where the center to center distance (between fluid streams) is 2.4 cm, the production rate did not show significant increase. This might be due to observed interference of the jets. Due to this interference, the jet from the spinning site (at the center) had a frequent stoppage and start up that eventually did not increase the production rate. Also such intermittent spinning caused streaming that increased the diameter distribution. With 5 pipettes where the center to center distance is 1.2 cm, it is observed that the adjacent fluid streams join together (due to branching) forming a single spinning site. This increases the flow rate, resulting in adverse effects: 1) droplets at edge drip from the plate while the jet is still spinning, resulting in intermittent spinning (eventually low production rate), and 2) such intermittent spinning causes streaming in every start up (that increases the average fiber diameter and its distribution). Thus, multiple

spinning sites using multiple pipettes on a single plate would be more successful at optimal center to center distance.

5.5 Spinning from multiple plates

Multiple jets could be also initiated by providing multiple spinning sites by utilizing more than one source plate. Several configurations were studied with different possible combinations of plates separated by 10 mm (up to four) as shown in Figure 4.3b and of multiple feed streams (up to three pipettes, spacing as mentioned in 5.4.3). In each configuration, the plates are treated with C_{10} and held at identical voltages with a feed rate of 45 µl/min (using a 2.0 mm pipette). In this configuration, the use of multiple pipettes provided multiple spinning sites on the first or topmost plate and then the fluid flowed down to subsequent plates, thus creating multiple spinning sites at each of four plates (cascade arrangement). However in all these configurations, it is noticed that the jets were more stable and continuous from the leading edges of the plates (in this case the bottom most plate) than other edges. In this section, this effect is discussed using electric field simulation. The effects of multiple plates and feed streams on fiber morphology and production rate are also discussed.

5.5.1 Electric field Simulation

Electric field magnitude was quantified (using Maxwell SV 2D simulation software) for multi-plate configuration. It is observed that the leading edge (in this case the bottom most plate in Figure 4.3b) has the highest electric field magnitude ($4.3 \pm 0.2 \times 10^5$ V/m) and the

steepest gradient compared to the other plate edges ($2.8 \pm 0.2 \times 10^5$ V/m). The field strength at the collector was $8.3 \pm 1.7 \times 10^4$ V/m (for an applied voltage of 32 kV). This complex electric field magnitude and gradient at the spinning sites, therefore, affect the jet initiation, jet profiles, and therefore, the average fiber diameter and diameter distribution. In the following sections these results and discussions of the multi-plate experiments are summarized. This result highlights the crucial importance of the electric field gradient at the edge of plate.

5.5.2 Experimental observations

Multi-plate experiments resulted in an intermittent electrospinning process (for both single and multiple feed streams) that followed a cycle; jet initiation by a pendent droplet, electrospinning, jet break-up by a subsequent droplet. This cycle is attributed to the excessive feed rate that under the current set up is required in order to feed to multiple plates. The jet break-up produced an intermittent spinning process which also resulted in occasional electrospraying or jet streaming. Spinning sites from bottommost plate edges have a strong electric field and gradient and display longer duration of the spinning cycle approximately 15 seconds of spinning with 2 seconds interval. On the other hand, at spinning sites where the electric field strength and gradient is relatively weak, jets initiated from a pendent droplet but vanished before it stabilized to spin; in other words, the interval was more than the spinning time.

Jets from the spinning sites at the bottommost plate edges displayed jet profiles similar to that of the single edge (due to similar electric field magnitude and gradient as single edge-plate) but jets from other spinning sites displayed shorter linear regions (~20%) and a smaller whipping cone angle (~30º full cone angle) with no secondary cone (due to less volume of liquid taken by the jet). All these variations contribute to producing larger average fiber diameters and a wider diameter distribution (290 ± 54 nm) for a working distance of 35 cm and 28 kV. Spinnability and porosity found to be 96.0% (due to intermittent spinning) and 69.0 ± 3.0 %, respectively.

5.5.3 Intermittent spinning in TNE

To better understand the intermittent electrospinning, a similar cycle (15 seconds of spinning with a two second interval) with TNE at 28 kV and a 35 cm working distance was studied. In such cases, nanofiber mat with some wet regions (caused by streaming) were obtained. The fiber diameter was found to be 325 ± 40 nm, which is relatively higher than that for the continuous TNE process (keeping all parameters the same) (292 ± 28 nm). Hence the increase in the fiber diameter (and diameter distribution) for the multiple-plate configuration can be attributed to the intermittent spinning and resultant streaming phenomenon.

5.5.4 Fabrication rate

In multi-plate experiments, four plates and three pipettes (offering 12 possible spinning sites) were employed. However a relatively low density of spinning sites is observed that produced an average of four jets at a given point of time. This is due to the intermittent process and the

difference in the electric field strength and gradient as discussed in 5.5.1. Fabrication rate for this configuration was found to be 0.153 gm/hr, lower than a two fluid streams from a single edge-plate. These results help to encourage investigating techniques with more focus on providing multiple spinning sites on a single edge-plate, or finding an optimum distance between plates where the electric field magnitude and gradient will be identical at all plates edges.

5. 6 Spinning from edge-cylinder

In this section, a new geometry, an extension of aforementioned concepts, edge-cylinder is introduced. Results of preliminary experiments using edge-cylinder geometry are summarized.

5.6.1 Experimental

Figure 5.9 shows an edge-cylinder set up. It consists of an aluminum bowl (similar to petri dish) of 8 cm in diameter of 0.5 cm thickness and 1.2 cm height that act as the positively-charged source and an aluminum hollow cylinder of 36 cm in diameter with 0.5 cm thickness and 10 cm height that act as a grounded collector, placed concentrically. Solution parameters are same as the one used for TNE and edge-plate experiments (i.e., poly(ethylene) oxide (M_w – 400, 000) at 6 wt % in de-ionized water). Polymer solution was filled in the bowl so that solution is in close contact with the edge of the bowl. For these preliminary experiments, an applied voltage of 14 kV was utilized.

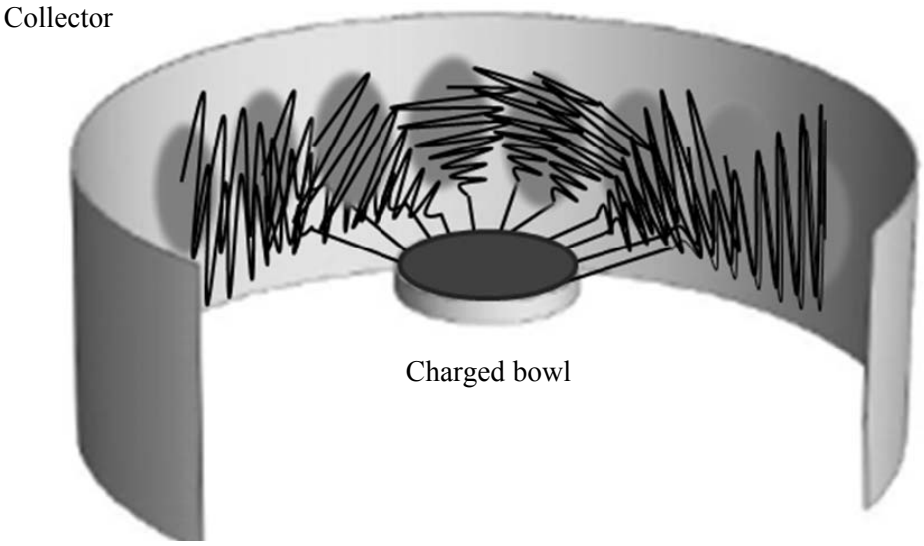

Figure 5.9 Representation of edge-cylinder electrospinning set up

5.6.2 Electric field simulation

Maxwell SV 2D was used to model the electric field distribution of the edge-cylinder geometry with a 15 kV and 15 cm working distance (from the surface of the source to the collector cylinder). Figure 5.10 shows the electric field distributions in edge-cylinder geometry as a planar cross-section. Electric field magnitude at the edge of the bowl was found to be $3.3 \pm 0.3 \times 10^5$ V/m and $6.8 \pm 2.2 \times 10^4$ V/m at the collector. Thus the edges of the bowl provide a strong electric field magnitude and gradient similar to TNE and edge-plate.

5.6.3 Preliminary results

In order to initiate the jets, a high voltage in magnitude and gradient (45 kV; i.e., $8.8 \pm 0.7 \times 10^5$ V/m) was required at the bowl edge.

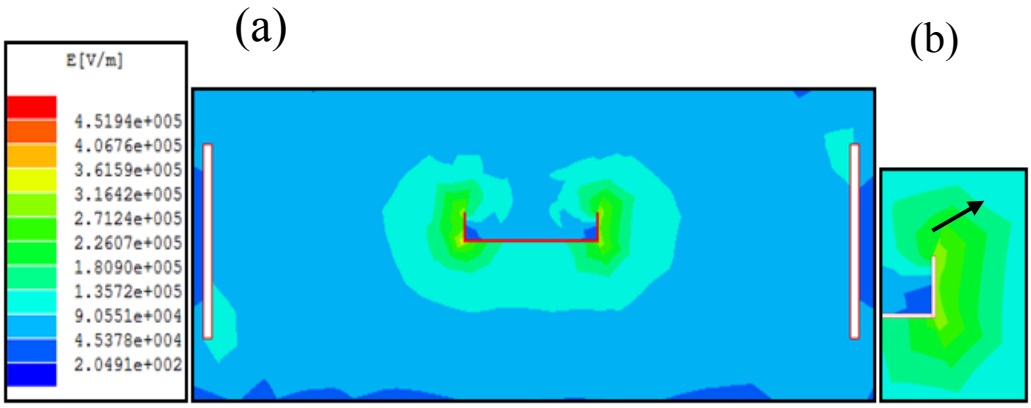

Figure 5.10 (a) Electric field distributions of edge-cylinder geometry (b) magnified image of the edge.

This is probably due to the absence of gravitational flow of fluid which (when falling) would thin down to a fine shape that assists in launching a jet. In edge-cylinder, upon application of this high voltage, the strong electric field at the edge of the bowl propels multiple jets along its edges (forming a radial pattern), however, at these field values, unfortunately, electrospraying to the collector. When the voltage is decreased to 14 kV ($3.3 \pm 0.3 \times 10^5$ V/m), continuous electrospinning was established. Approximately 30 jets were spinning radially from the edge of the bowl and fibers were deposited on to the cylindrical collector. These jets self-organized along the edges of the bowl, approximately equal distance between them. As well, the jets were propelling at an angle (~30º) from the bowl that more or less correlates with the observed pattern of electric field distribution (the arrow drawn in Figure 5.10b).

SEM Images of the edge-cylinder electrospun fibers is shown in Figure 5.11. Nanofibers sizes were measured to be 251 ± 25 nm, very similar to those formed under TNE. Also, as the working distance was short, no secondary whipping regions were observed (also similar to TNE). In addition, spinnability in edge-cylinder was 100% (excluding the initial electrospraying events). For future improvement, a method needs to be established to eliminate these initial electrospraying events, or present a new collector surface once the electrospinning starts.

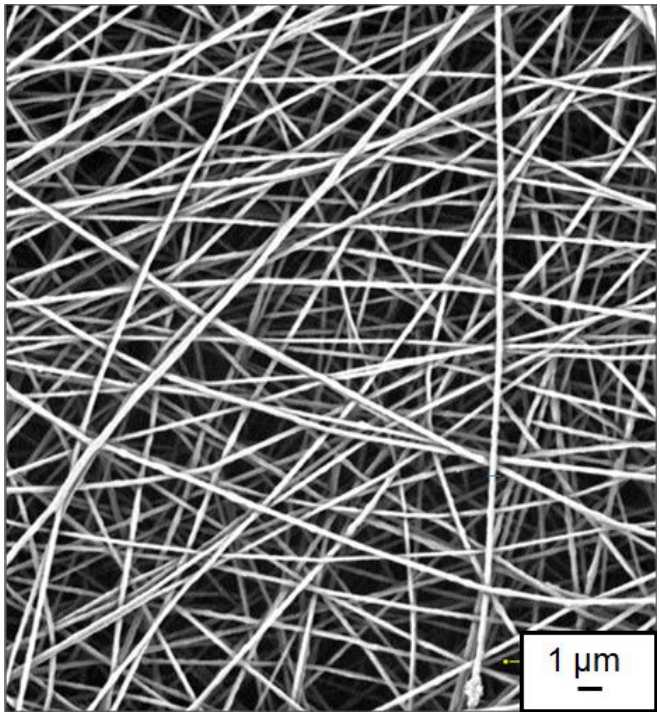

Figure 5.11 SEM image of edge-cylinder electrospun nanofibers (at 14 cm working distance and 14 kV)

Chapter 6

Conclusions

In this work, a simple geometry, edge-plate, is presented for fabricating nanofibers from gravity-assisted unconfined fluids. The edge-plate geometry provides a strong electric field magnitude and gradient at the spinning site similar to the needle-plate geometry (TNE), but a large area to accommodate multiple spinning sites and no aperture that can clog. The significance of electric field gradient as an important parameter for jet initiation is demonstrated with parallel plate geometry experiments.

Electrospun nanofibers from unconfined fluids using edge-plate geometry are similar in diameter (275 ± 32 nm) to that from TNE (243 ± 19.2 nm). Jet profiles including the linear and whipping regions showed similar trends in both geometries. At longer working distance, an extended whipping region is observed in both geometries. Properties of nanofibrous mat such as spinnability and porosity were investigated as a function of electric field strength and geometry and the process is stable over a range of experimental conditions.

Multiple jets were generated by using multiple fluid streams and/or multiple plate edges resulting in increased throughput. In one edge-plate set up with three fluid streams, the resultant throughput (0.27 g/hr) was approximately 10 times that of the TNE process (0.027 g/hr) at standard configurations. In such cases diameter of the nanofibers is not altered. In multiple edge-plate set up, the electric field magnitude and gradient were concentrated at the

bottommost edge thereby displaying relatively stable electrospinning only from these edges. Intermittent electrospinning was observed in this configuration, thereby affecting the average fiber diameter, diameter distribution and spinnability of the nanofibrous mats.

A preliminary investigation of edge-cylinder electrospinning is reported where ~ 30 jets were emanating and electrospinning from the source. Nanofibers from this geometry are very similar in morphology as that of the TNE. These results support the idea that fabrication of nanofibers at very high throughput can be achieved using geometries that are based on an edge (covered with an unconfined fluid) as a source, a potential approach that is free of clogging and complexity.

Chapter 7

Future work

This work investigated the prospect of simple edge-plate geometry for electrospinning from unconfined fluids. During this investigation, in order to reduce the variables, polymer solution properties such as conductivity, solvent, solvent proportion, were not modified. It would be highly interesting to investigate these variables in the proposed geometry.

Also this work presented the preliminary results from edge-cylinder geometry. Future work could be to optimize electrospinning from this geometry, particularly adding similar edges in a concentric fashion to further increase throughput or to develop multi component nanofibrous mats for specific applications.

Also it is recommended to identify and utilize sophisticated simulation software to analyze electric field distributions for different geometries. This could help to analyze in a three-dimensional view and also help in quantifying the electric field gradient.

REFERENCES

[1] Ramakrishna S, Fujihara K, Teo W, Lim T, Ma Z. An introduction to electrospinning and nanofibers. Singapore: World Scientific Publishing; 2005.

[2] Andrady AL. Science and technology of polymer nanofibers. USA: John Wiley & Sons, Inc., Publication; 2008.

[3] Huang ZM, Zhang YZ, Kotaki M, Ramakrishna S. A review on polymer nanofibers by electrospinning and their applications in nanocomposites. Composites Science and Technology 2003;63(15):2223-53.

[4] Schiffman JD, Schauer CL. A review: Electrospinning of biopolymer nanofibers and their applications. Polymer reviews 2008;48(2):317-52.

[5] Formhals A. Process and apparatus for preparing artificial threads. 1975504. 1934 Oct 2, 1934.

[6] Reneker DH, Chun I. Nanometer diameter fibers of polymer produced by electrospinning. Nanotechnology 1996;7:216-23.

[7] Tiwari MK, Yarin AL, Megaridis CM. Electrospun fibrous nanocomposites as permeable, flexible strain sensors. Journal of Applied Physics 2008;103(4):004305-1-10.

[8] McCullen S, Stevens D, Roberts W, Ojha S, Clarke L, Gorga R. Morphological, electrical, and mechanical characterization of electrospun nanofiber mats containing multiwalled carbon nanotubes. Macromolecules 2007:40(4):997-1003

[9] Freund M, Lewis N. A Chemically diverse conducting polymer-based electronic nose. Proc. Natl. Acad. Sci. U.S.A. 1995;92(7):2652-6.

[10] Filatov Y, Budyka K, Kirichenko V. Electrospinning of micro-and nanofibers: Fundamentals and applications in separation and filtration process. USA: Begell house, Inc.; 2007.

[11] Jirsak O, Sanetrnik F, Lukas D, Kotek V, Martinova L, Chaloupek J, inventors. A method of nanofibres production from a polymer solution using electrostatic spinning and a device for carrying out the method. WO2005024101. 2005.

[12] Yamashita Y, Ko F, Tanaka A, Miyake H. Characteristics of elastomeric nanofiber membranes produced by electrospinning. Journal of Textile Engineering 2007;53(4):137-42.

[13] Zhou F, Gong RH, Porat I. Mass production of nanofibre assemblies by electrostatic spinning. Polymer International 2009;58(4):331-42.

[14] Yarin AL, Zussman E. Upward needleless electrospinning of multiple nanofibers. Polymer 2004;45(9):2977-80.

[15] Formhals A, inventor. Method and apparatus for spinning. U.S. patent 2,160,962. 1939 .

[16] Formhals A, inventor. Artificial thread and method of producing same filed. U.S. patent 2,187, 306. 1940 .

[17] Formhals A, inventor. Producing of artificial fibers from fiber forming liquids. U.S. patent 2,323,025. 1943 .

[18] Formhals A, inventor. Method and apparatus for spinning. 2,349,950 patent. 1944 .

[19] Baumgarten PK. Electrostatic spinning of acrylic microfibers. Journal of Colloid and Interface Science 1971;36:71-9.

[20] Larrondo L, Manley RS. Electrostatics fiber spinning from polymer melts. Polymer Science : Part B : Polymer Physics 1981;19:909-20.

[21] Lukas D, Sarkar A, Martinova Lea. Physical principles of electrospinning (Electrospinning as a nano-scale technology of the twenty-first century). Textile progress 2009;41(2):59-140.

[22] Reneker DH, Chun I. Nanometre diameter fibres of polymer, produced by electrospinning. Nanotechnology 1996;7(3):216-23.

[23] Doshi J, Reneker DH. Electrospinning process and applications of electrospun fibers.. Journal of Electrostatistics 1995;35:151-60.

[24] Srinivasan G, Renker DH. Structure and morphology of small diameter electrospun aramid fibers. Polymer International 1995;36(2):195-201.

[25] Moghe AK, Gupta BS. Co-axial electrospinning for nanofiber structures: Preparation and applications. Polymer Reviews 2008;48(2):353-77.

[26] Ojha SS, Stevens DR, Stano KL, Hoffman TJ, Clarke LI, Gorga RE. Characterization of Electrical and Mechanical Properties for Coaxial Nanofibers with Poly(ethylene oxide) (PEO) Core and Multiwalled Carbon Nanotube/PEO Sheath. Macromolecules 2008;41:2509-13.

[27] Kim G, Cho YS, Kim WD. Stability analysis for multi jets electrospinning process modified with a cylindrical electrode.. European Polymer Journal 2006;42(9):2031-8.

[28] Yang Y, Jia Z, Liu J, Li Q, Hou L, Wang L, et al. Effect of electric field distribution uniformity on electropsinning.. Journal of Applied Physics 2008;103, 104307:1-11.

[29] Kim GH, Yoon H. A direct electrospinning process by combined electric field and air-blowing system for nanofibrous wound-dressings. Applied Physics A 2008;90(3):389-94.

[30] Deitzel JM, Kleinmeyer JD, Hirvonen JK, Beck Tan NC. Controlled deposition of electrospun poly(ethylene oxide) fibers. Polymer 2001;42(19):8163-70.

[31] Bellan LM, Craighead HG. Control of an electrospinning jet using electric focusing and jet -steering fields. Journal of Vacuum Science and Technology B ;24(6):3179-83.

[32] Secasanu VP, Giardina CK, Wang Y. A Novel Electrospinning Target to Improve the Yield of Uniaxially Aligned Fibers. Biotechnology Progress 2009;25(4):1169-75.

[33] Lee SJ, Cho NI, Lee DY. Effect of collector grounding on directionality of electrospun titania fibers. Journal of the European Ceramic Society 2007;27(13-15):3651-4.

[34] Teo WE, Ramakrishna S. A review on electrospinning design and nanofiber assemblies. Nanotechnology 2006;17:R89-R106.

[35] Taylor G. Electrically Driven jets. Proceedings of the Royal Society of London.Series A ,Mathematical and Physical Sciences 1969;313:453-75.

[36] Reneker DH, Yarin AL. Electrospining jets and polymer nanofibers. Polymer 2008;49(10):2387-425.

[37] Kong CS, Lee TH, Lee SH, Kim HS. Nano-web formation by the electrospinning at various electric fields. Journal of Materials Science 2007;42(19):8106-12.

[38] Fang D, Chang C, Hsiao BS, Chu B. Development of Multiple-Jet electrospinning technology. Polymeric nanofibers 2006;918:91-105.

[39] Yarin AL, Koombhongse S, Reneker DH. Taylor Cone and jetting from liquid droplets in electrospinning of nanofibers. Journal of Applied Physics 2001;90(9):4836-46.

[40] Rutledge GC, Fridrikh SV. Formation of fibers by electrospinning. Advanced Drug Delivery Reviews 2007;59:1384-91.

[41] Jaworek A, Krupa A. Classification of the modes of EHD Spraying. Journal of Aerosol Science 1999;30(7):873-93.

[42] Reneker DH, Yarin AL, Koombhongse HF. Bending instability of electrically charged liquid jets of polymer solutions in electrospinning.. Journal of Applied Physics 2000;87:4531-47.

[43] Reneker DH, Fong H editors. Polymeric Nanofibers. USA: American Chemical Society; 2005.

[44] Fong H, Chun I, Reneker DI. Beaded nanofibers formed during electrospinning. Polymer 1999;40(16):4585-92.

[45] Tan SH, Inai R, Kotaki M, Ramakrishna S. Systematic parameter study for ultra-fine fiber fabrication via electrospinning process. Polymer 2005;46:6128-34.

[46] Thompson CJ, Chase GG, Yarin AL, Reneker DH. Effects of parameters on nanofiber diameter determined from electrospinning model. Polymer 2007;48:6913-22.

[47] Heikkila P, Harlin A. Parameter study of electrospinning of polyamide -6. European Polymer Journal 2008;44:3067-79.

[48] Varesano A, Carletto RA, Mazzuchetti G. Experimental investigations on the multi-jet electrospinning process.. Journals of Materials Processing Technology 2009;209(11):5178-85.

[49] Maheshwari S, Chang HC. Assembly of Multi-Stranded Nanofiber threads through AC Eletrospinning. Advanced Materials 2009;21:349-54.

[50] Kessick R, Fenn J, Tepper G. The use of AC potentials in electrospraying and electrospinning processes. Polymer 2004;45:2981-4.

[51] He JH. A Mathematical Model for AC-Electrospinning. International Journal of Nonlinear Sciences and Numerical Simulations 2005;6(3):243-8.

[52] Hur S, Kim WD. The Electrospinning Process and Mechanical Properties of Nanofiber Mats under Vacuum Conditions. Key Engineering materials 2006;326-328:393-6.

[53] Sarkar S, Deevi S, Tepper G. Biased AC Electrospinning of Aligned Polymer Nanofibers. Macromolecule Rapid Communications 2007;28:1034-9.

[54] Yu J, Fridrikh S, Rutledge G. The role of elasticity in the formation of electrospun fibers. Polymer 2006;47(13):4789-97.

[55] Kilic A, Oruc F, Demir A. Effects of polarity on electrospinning process. Text.Res.J. 2008;78(6):532-9.

[56] Supaphol P, Mit-Uppatham C, Nithitanakul M. Ultrafine electrospun polyamide-6 fibers: Effect of emitting electrode polarity on morphology and average fiber diameter. Journal of polymer science.Part B, Polymer physics 2005;43(24):3699-712.

[57] De Vrieze S, Van Camp T, Nelvig A, Hagstrom B, Westbroek P, De Clerck K. The effect of temperature and humidity on electrospinning. Journal of Materials Science 2009;44(5):1357-62.

[58] Tong H, Wang M. Effects of processing parameters on the morphology and size of electrospun PHBV micro- and nano-fibers. Key engineering materials 2007;334-335:1233-6.

[59] Deitzel J, Kleinmeyer J, Harris D, Tan N. The effect of processing variables on the morphology of electrospun nanofibers and textiles. Polymer 2001;42(1):261-72.

[60] Wang T, Kumar S. Electrospinning of Polyacrylonitirile nanofibers. Journal of Applied Polymer Science 2006;102(2):1023-9.

[61] Brown P, Stevens K. Nanofibers and nanotechnology in textiles. Cambridge; Boca Raton, FL: Woodhead; CRC Press; 2007.

[62] Burger C, Hsiao B, Chu B. Nanofibrous materials and their applications. Annual review of materials research 2006;36(1):333-68.

[63] Zhou F, Gong R, Porat I. Three-jet electrospinning using a flat spinneret. Journal of Materials Science 2009;44(20):5501-8.

[64] Wang X, Niu H, Lin T, Xungai Wang. Needleless electrospinning of nanofibers with a conical wire coil. Polymer Engineering and Science 2009;49(8):1582-6.

[65] Vaseashta A. Controlled formation of multiple Taylor cones in electrospinning process. Applied Physics Letters 2007;90, 093115.

[66] Paruchuri S, Brenner MP. Splitting of a liquid jet. Physical Review Letters 2007;98, 134502(13).

[67] Bowman J, Tayor M, Sharma V. Multispinneret methodologies for high throughput electrospun nanofiber. Materials Research Society Symposiums Proceedings; 2003.

[68] Theron SA, Yarin AL, Zussman E, Knoll E. Multiple jets in electrospinning: experiment and modeling. Polymer 2005;46(9):2889-99.

[69] Tomaszewski W, Szadkowski M. Investigation of electrospinning with the use of a multi-jet electrospinning head. Fibres & Textiles in Eastern Europe 2005;13(4):22-6.

[70] Yang Y, Jia Z, Li Q, Hou L, Gao H, Wang L. Experimental investigation of the governing parameters in the electrospinning of polyethylene oxide solution.. 8th International Conference on properties and applications of dielectric materials, IEEE transactions on dielectrics and electrical insulation 2006;13:580-5.

[71] Kim HY, inventor. A bottom-up electrospinning devices, and nanofibers prepared by using the same. WO20050073441. 2005 .

[72] Kim HY, Park JC. Conjugate electrospinning devices, Conjugate nonwoven and filament comprising nanofibers prepared by using the same. WO2007035011. 2007 .

[73] Dosunmu OO, Chase CG, Kataphinan W, Reneker DH. Electrospinning of polymer nanofibers from multiple jets on a porous tubular surface. Nanotechnology 2006;17(4):1123-7.

[74] Varabhas JS, Chase GG, Reneker DH. Electrospun nanofibers from a porous hollow tube. Polymer 2008;49(19):4226-9.

[75] Andray AL, Ensor DS, Newsome RJ, inventors. Electrospinning of fibers using a rotatable spray head. US 2006/0228435. 2006 Oct 12, 2006.

[76] Srivastava Y, Marquez M, Thorsen T. Multijet electrospinning of conducting nanofibers from microfluidic manifolds. Journal of Applied Polymer Science 2007;106:3171-8.

[77] Salem DR. Electrospinning of nanofibers and the charge injection method. Nanofibers and Nanotechnology in Textiles,. In: Brown PJ, Stevens K, editors. Cambridge.: Woodhead Publishing; 2007.

[78] Lukas D, Sarkar A, Pokorny P. Self-organization of jets in electrospinning from free liquid surface: A generalized approach.. Journal of Applied Physics 2008;103; 084309.

[79] Liu Y, He J. Bubble electrospinning for mass production of nanofibers. . International Journal of Nonlinear Sciences and Numerical Simulations 2007;8(3):393-6.

[80] Weitz RT, Harnau L, Rauschenbach S, Burghard M, Kern K. Polymer nanofibers via nozzle-free centrifugal spinning. Nano Letters 2008;8(4):1187-91.

[81] Mathauer K, Frank CW. Binary Self-Assembled Monolayers As Prepared by Successive Adsorption of Alkyltrichlorosilanes. Langmuir 1993;9(12):3446-51.

[82] Ulman A. Self-Assembled Monolayers of Alkyltrichlorosilanes : Building Blocks for Future Organic Materials. Advanced Materials 1990;2(12):573-82.

[83] Ulman A. Formation and Structure of Self-Assembled Monolayers. Chemical Reviews 1996;96(4):1533-54.

[84] Ulman A. Self Assembled Monolayers of thiols. : Academic Press; 1998.

[85] D. Stevens. Molecular Dynamics in Self-assembled Monolayers and Polymers Studied via sensitive Dielectric Spectroscopy; 2009.

[86] Ferguson G.S., Chaudhary M. K., Biebuyck H.A., Whitesides G.M. Monolayers on Disordered Substrates: Self- Assembly of Alkyltrichlorosilanes on Surface-Modified Polyethylene and Poly(dimethylsiloxane). Macromolecules 1993(26):5870-5.

[87] Niu Haitao, Lin Tong, Wang Xungai. Needleless electrospinning. I. A comparison of cylinder and disk nozzles.. Journal of Applied Polymer Science 2009;114(6):3524-30.

[88] Shin YM, Hohman MM, Brenner MP, Rutledge GC. Experimental characterization of electrospinning: the electrically forced jet and instabilities. Polymer 2001;42(25):9955-67.

[89] Cengiz F, Krucinska I, Gliscinska E, Chrzanowski M, Goktepe F. Comparative analysis of various electrospinning methods of nanofibre formation.. Fibres & Textiles in Eastern Europe 2009;17(1):13-9.